

Optical Simulation and Optimization of Light Extraction Efficiency
for Organic Light Emitting Diodes

by

Hang Su

A Thesis Presented in Partial Fulfillment
of the Requirements for the Degree
Master of Science

Approved April 2016 by the
Graduate Supervisory Committee:

Liping Wang, Chair
Jian Li
Huei-ping Huang

ARIZONA STATE UNIVERSITY

May 2016

ABSTRACT

Current organic light emitting diodes (OLEDs) suffer from the low light extraction efficiency. In this thesis, novel OLED structures including photonic crystal, Fabry-Perot resonance cavity and hyperbolic metamaterials were numerically simulated and theoretically investigated. Finite-difference time-domain (FDTD) method was employed to numerically simulate the light extraction efficiency of various 3D OLED structures. With photonic crystal structures, a maximum of 30% extraction efficiency is achieved. A higher external quantum efficiency of 35% is derived after applying Fabry-Perot resonance cavity into OLEDs. Furthermore, different factors such as material properties, layer thicknesses and dipole polarizations and locations have been studied. Moreover, an upper limit for the light extraction efficiency of 80% is reached theoretically with perfect reflector and single dipole polarization and location. To elucidate the physical mechanism, transfer matrix method is introduced to calculate the spectral-hemispherical reflectance of the multilayer OLED structures. In addition, an attempt of using hyperbolic metamaterial in OLED has been made and resulted in 27% external quantum efficiency, due to the similar mechanism of wave interference as Fabry-Perot structure. The simulation and optimization methods and findings would facilitate the design of next generation, high-efficiency OLED devices.

DEDICATION

To

MY PARENTS

Juan Zhang and Dongyi Su

MY GRANDPARENTS

Yuzhen Liu and Yunxing Su
Yushan Zhang and Lianying Xia

ACKNOWLEDGMENTS

First of all, I would like to express deepest gratitude to my advisor Dr. Liping Wang, for his expert advice and encouragement throughout the research. I am very grateful for the opportunity to work in his research group. Not only did he give me mentorship in academic aspect, but he also taught me the way of thinking and affected my personality. I would also like to offer my sincere appreciation to Dr. Jian Li and Dr. Huei-Ping Huang, who devoted their valuable time to serve as my committee member and provided valuable advice.

I would also like to thank my group members Hao, Ray, Yue, Hassan, Sydney, Payam and Xiaoyan, for their help and support. I learned a lot during collaborating and interacting with them during my Master study. I want to specially thank Hao for his help at the beginning and during my research. I am also very grateful to Jeremy, who is a former PhD student in Dr. Jian Li's group, for the research results in his dissertation.

Last but not least, I want to dedicate this thesis to my dearest family. They kept encouraging me when I encountered difficulty during the writing process of this thesis. Without the support and encouragement from them, I could never finish my Master study. Finally, I want to express my appreciation to my boyfriend Jason, for all his love and support during my Master study.

TABLE OF CONTENTS

	Page
LIST OF TABLES.....	vii
LIST OF FIGURES.....	viii
CHAPTER	
1 BACKGROUND AND INTRODUCTION.....	1
1.1 Motivation	1
1.2 About OLED.....	2
1.2.1 OLED Introduction.....	2
1.2.2 Efficiency Enhancement Methods	4
1.3 About FDTD.....	5
2 3D SIMULATION METHODOLOGY IN FDTD SOLUTION	8
2.1 Simulation Processes	8
2.2 Geometry Model.....	8
2.3 Simulation Domain and Analysis Monitor.....	13
2.4 Meshing.....	18
2.5 Convergence Check.....	20
2.6 Sweep Tool	21
3 PHOTONIC CRYSTAL SRUCTURE.....	23
3.1 Introduction.....	23
3.2 Results and Discussion.....	25
3.3 Effect of Dispersive Optical Constants of Materials.....	26

CHAPTER	Page
4 FABRY-PEROT RESONANCE CAVITIES	28
4.1 Simulation Setup.....	28
4.2 Factors That Affect Spectrum Extraction.....	29
4.2.1 Different Materials for Anode Layer	29
4.2.2 Thickness of the Anode Layer	30
4.2.3 Field Concentration Effect	32
4.2.4 Thickness of NPD Layer.....	34
4.2.5 Dipole Polarizations and Locations	35
4.2.6 Ray Tracing Method.....	36
4.2.7 Perfect Reflector as Cathode	38
5 ELUCIDATING PHYSICAL MECHANISM WITH ANALYTICAL MODEL.....	41
5.1 Transfer Matrix Method.....	41
5.2 Comparison Between Analytical Model and Numerical Model	43
6 HYPERPOLIC METAMATERIAL	46
6.1 Introduction.....	46
6.2 Results and Analysis.....	48
7 CONCLUSIONS AND FUTURE WORK.....	51
REFERENCES	53
APPENDIX.....	55
A MATERIAL REFRACTIVE INDICES	55

APPENDIX

Page

B	FDTD CODE	60
B.1	MODEL SETUP.....	61
B.2	FAR FIELD ANALYSIS GROUP.....	64
B.3	BOX TRANSMISSION MONITOR.....	69
B.3.1	SETUP	69
B.3.2	CALCULATION SCRIPT.....	71
B.4	SWEEP TOOL SCRIPT	72

LIST OF TABLES

Table	Page
1. Example of Setup Code.....	11
2. Different Materials of Metal Layer and Corresponding Simulation Results.....	29
3. Different Thicknesses of Silver Layer and Corresponding Simulation Results.....	30
4. Different Thicknesses of Gold Layer and Corresponding Simulation Results.....	31
5. Varies Thicknesses of NPD Layer and Corresponding Simulation Results.....	34

LIST OF FIGURES

Figure	Page
1. Organic LED Main Components	3
2. Numerically Predicted Energy Losses and Measured Quantum Efficiency of a Red Bottom OLEDs as a Function of the Electron Transport Layer	4
3. Flow Chart for the FDTD Simulation of OLEDs.....	8
4. Schematic of a Conventional Organic LED Structure	9
5. View of the Main Interface (3D Modeler Window and the Objects Tree).....	9
6. Window of “Model -- Edit Object-- Setup User Properties”.....	10
7. Material Edit Window.....	12
8. Material Explorer Window to do Material Fit and Plot	13
9. Boundary Conditions Setup Window	15
10. Schematic Numerical Model in FDTD.....	15
11. Analysis Group for (a) Far-Field Emission and (b) Dipole Power Calculation	16
12. Mesh Setting Window for the Whole Domain.....	19
13. Edit Window for Override Mesh.....	20
14. Major Convergence Factors that Ensures the Numerical Accuracy in FDTD Simulations for OLEDs.....	20
15. Setup Dipole Location and Numbers in Sweep Tool	22
16. Schematic of Photonic Crystal Structure OLED.....	24
17. Mechanism of Losses in OLED Structure.....	24
18. Results of Photonic Crystal Structures	25

Figure	Page
19. Comparison Between Two Simulation Results under Zero DBR pair and NPD Thickness 40nm.	27
20. Proposed Fabry-Perot Cavity OLED	28
21. Spectrum Extraction Efficiency of Different Cases Above (table 2)	29
22. Spectrum Extraction Efficiency of Different Cases Above (table 3).....	31
23. Spectrum Extraction Efficiency of Different Cases Above (table 4).....	32
24. Comparison of ITO Structure with Fabry-Perot Structure Device (a) Extraction Efficiency of ITO Structure (b) Extraction Efficiency of Fabry-Perot Structure (c) Electric Field of Different Structure at Different Wavelength	33
25. Spectrum Extraction Efficiency of Different Cases Above (table 5).....	35
26. Light Extraction Efficiency of a Single Dipole at Different Conditions	36
27. Schematic of the Ray Tracing Method Calculation	37
28. Comparison Results of Single Dipole With and Without Ray-Tracing Method.....	38
29. Light Extraction Efficiency of Fabry-Perot Structure Simulated using Palik Data, Drude Model and Perfect Reflector Model for Al layer.....	40
30. Comparison Between the Light Extraction Efficiency and Reflectance.....	44
31. k-space Topology	47
32. Schematic of Multilayer Hyperbolic Metamaterial.....	47
33. Material Type Predicted by Effective Medium Theory.....	48
34. Simulation Results using Multilayer HMM and EMT Method HMM	49
35. Comparison of Results from HMM Structure and Fabry-Perot Structure OLED	50

Chapter 1

BACKGROUND AND INTRODUCTION

1.1. Motivation

In 2014, the U.S. Energy Information Administration (EIA) estimated that roughly 412 billion kWh of electricity generated in the United States were consumed for lighting by both residential and commercial sectors. This comprises 11% of U.S. total electricity usage. This can be translated into an equivalent of \$29 billion dollars per year assuming an average power plant efficiency of 30% and fuel price of \$40/barrel of crude oil. Similarly, it is equivalent to 374 billion kg of CO₂ emission per year.

Several lighting methods nowadays are incandescent light bulb, halogen lamp and solid state light. Incandescent light bulb generates light by passing electric current through a resistance-Tungsten. Therefore, Tungsten increases to a very high temperature (around 2500K). It then radiates heat over a broad range of wavelength including 400nm-700nm (visible light range) based on Wien's law. In this way, incandescent light bulb converts less than 5% of electrical power input into visible light. Similar physical concept stands behind halogen lamp except that the tungsten filament evaporation is prevented by a chemical reaction which helps increasing its life. Tungsten filament and halogen gas together can form a halogen cycle chemical reaction which will redeposit evaporated tungsten back on to the filament. Solid state lighting (SSL) has arisen as a relatively new technology of lighting. When a proper voltage is applied to light emitting diode (LED), electrons tends to recombined with electron-holes and release energy in form of photon. LED has achieved most of lighting basic objectives such as efficiency, color rendering, lifetime, and being environmentally friendly. Nevertheless, Performance of LED depends on ambient temperature, which may lead to a device failure eventually if the heat sink failed to reject enough heat. Besides other disadvantages such as light

quality and voltage sensitivity, capital cost of LED is one of the most disadvantages LED which is considered high relative to other lighting types such as incandescent and fluorescent light bulbs. Unlike traditional LEDs, Organic LED is a surface light source. OLED is made of a very thin organic layer, which makes it more flexible, thinner and lighter than LED.

OLED is a promising new lighting technology for lightings in general applications and large flat panel displays especially. OLED is anticipated to provide a better coloring picture for TVs and smartphones with less energy consumption and lower manufacturing cost. However, conventional OLED has a relatively low efficiency around 20%. For that reason, this thesis investigates the potential of increasing the extraction efficiency of OLED using different configurations.

1.2. About OLED

1.2.1. OLED introduction

Organic light emitting diode (OLED) is a type of Light Emitting Diode (LED) which emits visible light in response to an electric current. Different from LED, the electroluminescent layer of OLED is made of organic material. In recent years, OLED plays an increasing important role in flat panel displays and lighting applications. Without using backlight, OLED can display deeper black levels than Liquid crystal display (LCD). Moreover, thinner appearance, better performance as well as its flexibility make OLED more competitive to other display device.

OLED primarily consists of organic emitting layer sandwiches by a metal layer (cathode) and a transparent conducting oxide layer (anode). A substrate is needed and usually made of glass or plastic. Principle of the device is showed schematically in figure 1 below.

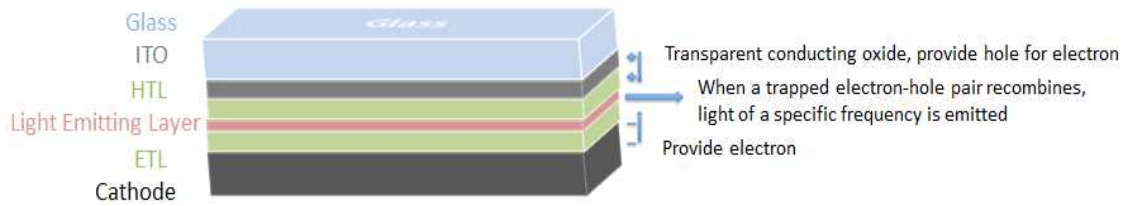


Figure 1: Organic LED Main Components

where HTL indicates “Hole transport layer” and ETL indicates “Electron transport layer”. The organic light emitting layer in between generates light through the radiative decay of molecular excited states (excitons). Total efficiency of the OLED device is impact by the internal quantum efficiency and light extraction efficiency.

$$QE = IQE \times LEE \quad (1)$$

where Internal Quantum Efficiency (IQE) represents the percentage of electron-hole recombination that radiates photons; LEE= Light Extraction Efficiency, which is the ratio of extracted photon to total generated photons; QE= Total Quantum Efficiency.

In conventional structure of OLED nowadays, light extraction efficiency is only around 20%. In contrast, by using electro-phosphorescent materials with proper management of singlet and triplet excitons, internal quantum efficiency of organic electroluminescent devices has reached about 100%. Therefore, more and more researchers are making efforts to enhance the light extraction efficiency of the OLED. Figure 2 below shows the mechanism of energy losses in a red phosphorescent OLED device. Radiative losses consist of absorption losses, surface plasmons losses, waveguided losses and losses due to the substrate.

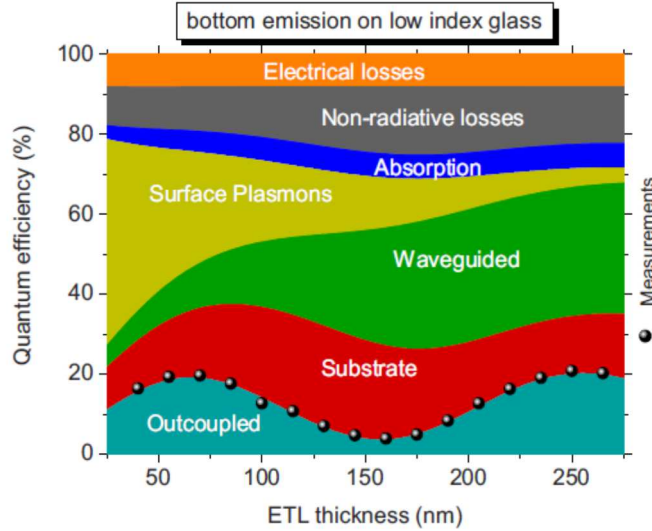


Figure 2: Numerically Predicted Energy Losses and Measured Quantum Efficiency of a Red Bottom OLEDs as a Function of the Electron Transport Layer

Substrate losses are mainly because of the total internal reflectance (TIR) on the air and glass interface. This can be avoided by surface modifications. Waveguided mode is also due to the TIR but inside the structure. Faby-Perot and Photonic Crystal structures are applied to decrease waveguided losses (Chapter 3,4). Surface Plasmon (SP), however, is the electromagnetic wave excited by evanescent wave at an interface between a dielectric material and metallic material. Surface Plasmon Polariton (SPP) only propagates along the surface, thus can not extracted out of the Organic LED device. In this thesis, Hyperbolic Metamaterial is researched for the purpose of transferring evanescent wave to propagating wave. Absorption losses due to the extinction coefficient of metallic materials can be reduced by engineering non-loss metallic material. Although absolute non-loss metallic material can not be achieved, simulations with this material (Section 4.2.7) can give the upper limit extraction efficiency of Oraganic LEDs.

1.2.2. Efficiency enhancement methods

In conventional OLED, 80% of the emitting light is trapped by the structure due to different mechanisms (section 1.2.1). To achieve higher thermal emission, various

techniques have been applied to reduce those losses. Encountering a rough surface is considered one of the simplest and most effective techniques to reduce the substrate losses. For wave-guided modes, light trapped at substrate/air interface extracts out because of the scattering effect after increasing the surface roughness. This method increased the extraction efficiency of some structures to 50%. Another cost effective technique is using texturing meshed substrate surfaces, which leads to an over 30% increase in extraction efficiency. Modifying the substrate can only help reduce the energy loss from glass and air interface. Lots of progresses have been made to deal with total internal reflectance among the organic layers and ITO layer. For example, Wang et al. highly improved the efficiency of green organic LEDs by using plastic substrate, Ta_2O_5 optical coupling layer, gold anode layer and MoO_3 as hole-injection layer. A maximum external quantum efficiency of 63% has been achieved with green OLEDs. In addition, one of the most promising techniques is plasmonic-grating OLEDs. Fabricate nano-structured dielectric grating on the metal film can help convert the guided wave to radiated wave through excitation of SPs. Research showed that hexagonal gratings are better than rectangular gratings in efficiency enhancement.

Simulation methods used in those researches are mostly analytical and experimental methods. In this thesis, numerical method based on FDTD solutions is applied, which can be used to further study the electric field in glass layer, as well as the extraction efficiencies of dipoles on different locations and polarizations.

1.3. About FDTD

FDTD Solutions is a 3D Maxwell solver designed by Lumerical Solutions, Inc.. It can be utilized for analyzing the interaction of UV, visible and IR radiation with complicated geometries. To optimize the quantum efficiency of Organic LEDs, it is

essential to investigate how the electromagnetic wave propagating in the structure. It's challenging to calculate the effects of these structures and patterns without building prototypes. However, building prototypes is expensive and time-consuming. Instead, FDTD can cheaply and quickly test the design and solve the problem.

Geometry model of OLED can be constructed using different shape of objects in FDTD. For gratings or other repeated components in FDTD, structure group can be applied. EM wave within visible range is generated in the emitting layer when a trapped electron-hole pair recombines. This process is known as spontaneous emission. The photons are of random directions, phases and polarizations. Therefore, using electromagnetic point dipole sources to simulate the generated light is feasible. Because FDTD is a coherent simulation method, 3 separate simulations of the same dipole oriented along the x, y and z axes must be run and sum up incoherently.

$$\langle |\vec{E}|^2 \rangle = \frac{1}{3} \left[|E_x|^2 + |E_y|^2 + |E_z|^2 \right] \quad (2)$$

where E_x, E_y, E_z are the electromagnetic fields generated by one single dipole along x, y, z directions.

PML boundaries should be used in the simulation, which means fields absorbed by boundaries cannot make it into the far field. In contrast, periodic boundaries may lead to interference from neighboring dipoles.

Power transmission box is used to get the emitted power from a dipole. The box should be large enough such that monitors do not overlap with source injection region, but small enough such that only a small amount of power is absorbed inside the region. The glass substrate is usually very thick, so the interface of glass-air cannot be directly modeled in the FDTD. Therefore the far field projection functions are chosen to simulate the reflection and refraction effects on this interface.

Light Extraction Efficiency (LEE) is defined as optical power escapes into the air versus power generated in the emitting layer of the OLED.

$$QE = \frac{\gamma_{rad} + \gamma_{abs}}{\gamma_{rad} + \gamma_{nr} + \gamma_{abs}} \cdot \frac{\gamma_{rad}}{\gamma_{rad} + \gamma_{abs}} = IQE \cdot LEE \quad (3)$$

where γ_{rad} is the EM decay to the far field, γ_{abs} is the EM decay which absorbed in the device, γ_{nr} is the Non EM decay. All of those unknowns can be derived from FDTD based simulation except for γ_{nr} . Detailed simulation processes are presented in Chapter 2.

Chapter 2

3D SIMULATION METHODOLOGY IN FDTD SOLUTION

2.1. Simulation Processes

The finite-difference time-domain (FDTD) method is an advanced method to solve Maxwell's equations in irregular and complex geometries. The following chapter shows the 3D simulation methodology using FDTD to solve Light Extraction Efficiency for an OLED structure. Figure 2 shows the flow chart for OLED simulation in FDTD.

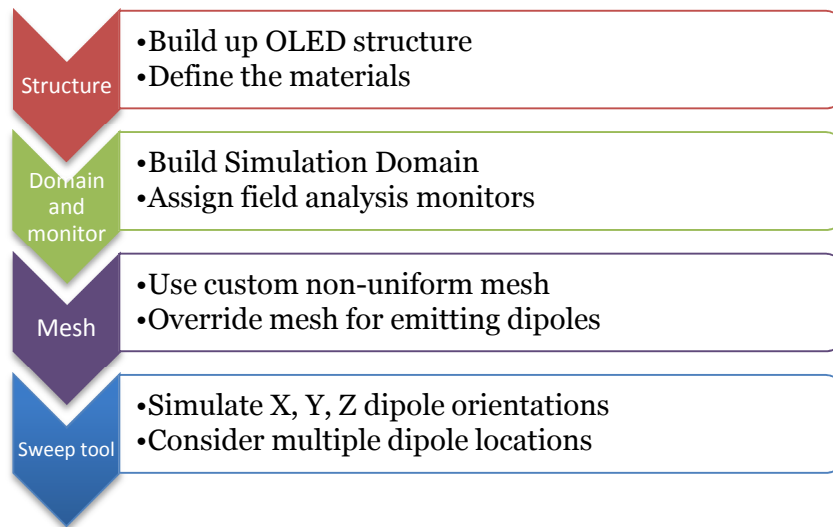


Figure 3: Flow Chart for the FDTD Simulation of OLEDs

2.2 Geometry Model

In this section, the multilayer structure below is used as an example.

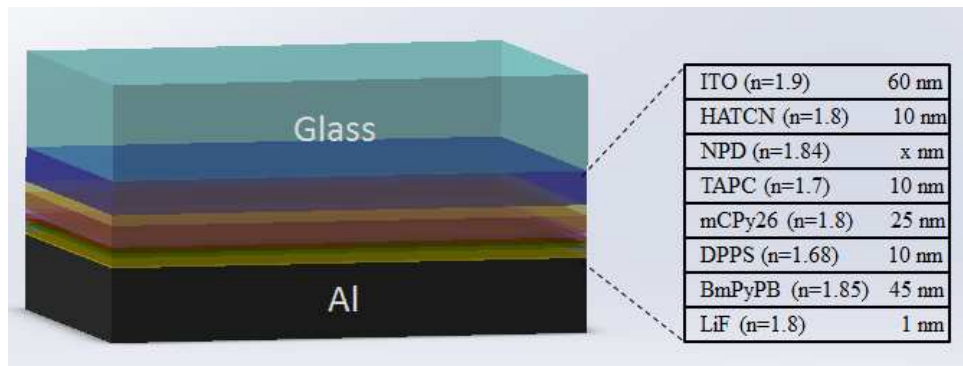


Figure 4: Schematic of a Conventional Organic LED Structure

where mCPy26 ($n=1.8$) is the emitting layer. Note that in this structure, the extinction coefficients (k) for all layers are small enough to be considered as 0, except for the substrate layer Al. The material properties of Al are defined using the Palik data.

1) Create the structure.

After getting started by double click “Numerical -- FDTD Solutions”, it is necessary to create the structure for the OLED device.

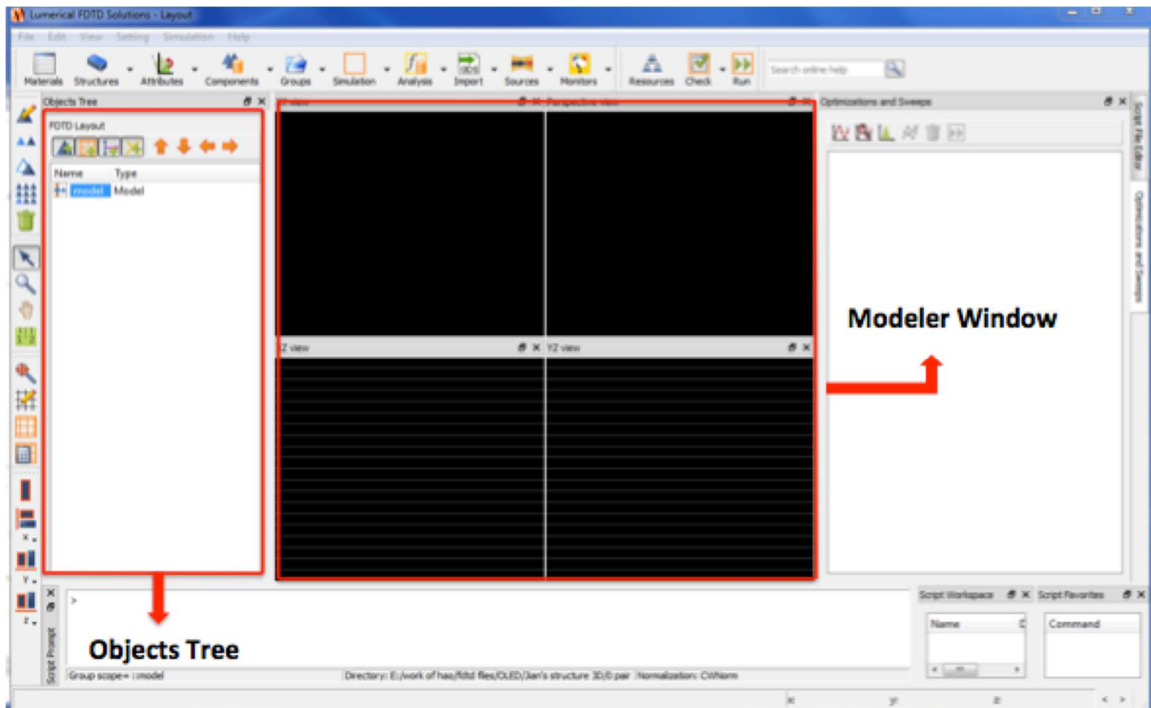


Figure 5: View of the Main Interface (3D Modeler Window and the Objects Tree)



Click the icon “Structures”, which is above the objects tree, to add rectangular Layers into the structure. 10 layers are needed to be built in this case, so click 10 times on this icon and import those layers. Right click on the rectangle structure inside the objects tree, and click “Edit Object Window” to rename the layers.

Next step is to define its dimensions and properties. This can be done in two ways: one is using Edit object Window by right click each layer in the objects tree, the other is writing “setup script” in ‘model’. Note that the setup script will always have the top priority of implement. In this guide, setup script is used to define all the dimensions and Edit object Window to define the material properties.

2) Setup the dimensions of the structure.

Firstly, define user properties. Right click “model”, and open “Edit object” window. Then go into the “Setup-- Variables” menu, and click “Add” icon next to the “User properties” and import variable name, type, value and Units.

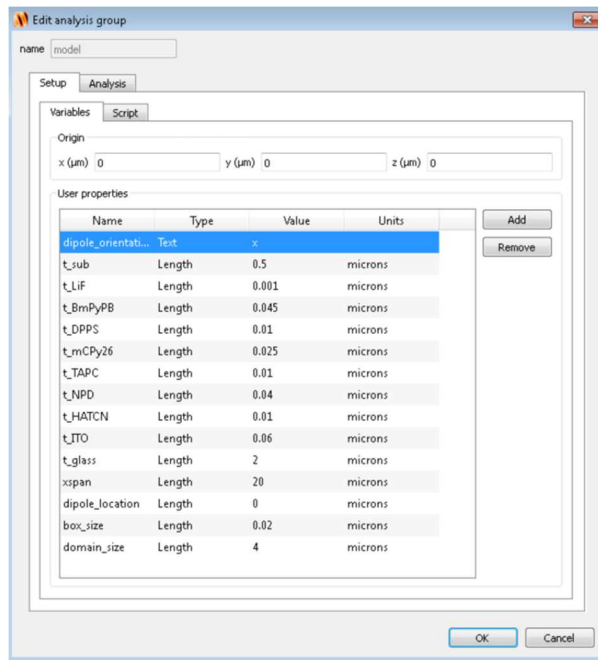


Figure 6: Window of “model -- Edit Object-- setup user properties”

Secondly, open the “Setup—Script” menu in the same window and write code in it to define the structure. Take substrate layer as an example:


Code	Comments
<code>select("substrate");</code>	<code>#Select the layer you want to setup</code>
<code>set('x',0);</code>	<code>#Set x location</code>
<code>set('x span', xspan);</code>	<code>#Set the length of x direction as "xspan", which is defined in the previous "user properties".</code>
<code>set('y',0);</code>	<code>#Set y location</code>
<code>set('y span', xspan);</code>	<code>#Set the length of y direction as "xspan"</code>
<code>set('z min', -0.5*10^-6);</code>	<code>#Set the lower boundary of z direction</code>
<code>set('z max', t_sub-0.5*10^-6);</code>	<code>#Set the upper boundary of z direction</code>

Table 1: Example of Setup Code

Similarly, setup other the location and dimension of other 10 layers. After writing the code, click "test" icon at the right lower corner of the "setup script" to test the validity of the code. Model setup script for this particular case is showed in Appendix 1.

3) Add light source in the structure

Light is generated in the emitting layer of an Organic LED when the injected electrons and holes recombine and create photons (spontaneous emission). It is possible to treat the generated light classically using electromagnetic point dipole sources. Select

"dipole" source in the menu under  "Sources" icon, which is on top of the FDTD main interface. Then, use "model--setup--script" to define its location and orientation. Same method with which defining the geometry of structures (Appendix A).

Because photons are spontaneously emitting in the active layer, different locations and orientations of dipoles are need to be simulated separately and take average to get the final result. Section 2.6 will explain how to use the sweep tool to average the results from different dipole simulations.

4) Define Material properties of each layer

To define the material properties of each layer, click Material menu in the same Edit Object Window. When it is dielectric material with constant index, n value (a.k.a

refractive index) can be input directly into the “index” column. Use the same method to define every layer which has constant index along all wavelengths.

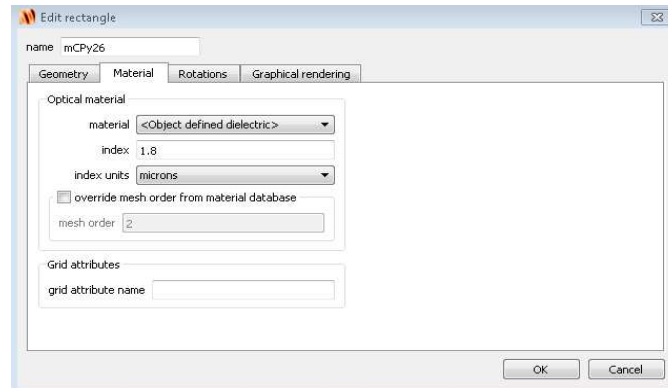



Figure 7: Material Edit Window

To define wavelength dependent material, click and open “material” menu above index column. In this case, “Al (Aluminum) - Palik” data is used to define substrate layer. Manipulation of fit and plot the material index is needed, since complex index data is not continued in the Material Database in this case. FDTD use polynomial equations depend on wavelength to define the index n (refraction index) and k (extinction coefficient). We need to change the “fit Tolerance” and “max coefficients” to fit the data points. Click “” icon on the top left corner of FDTD, then click “Go to Material Explorer” button on the left bottom corner, define fit Tolerance and max coefficients and click “Fit and plot” to check whether the plot is match.

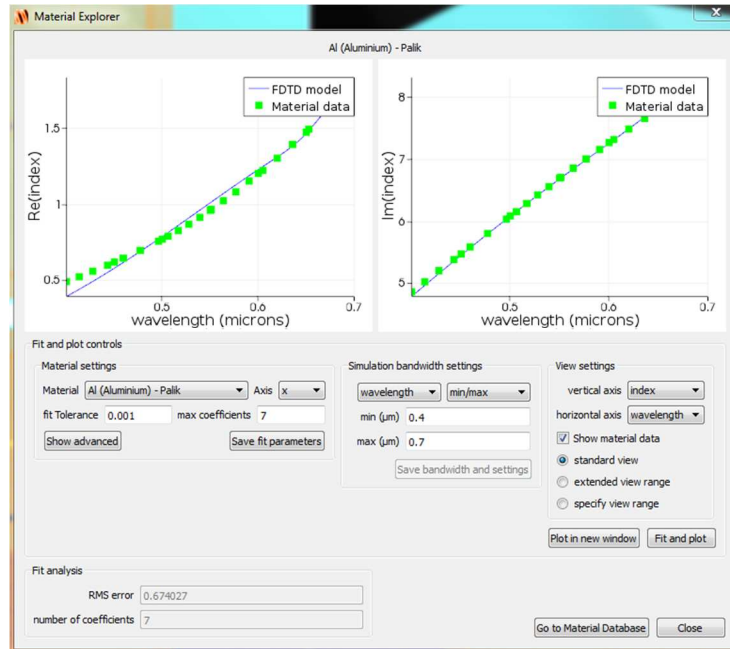


Figure 8: Material Explorer Window to do Material Fit and Plot

Al (Palik) experiment data are attached in the FDTD software. However, These experiment or calculated material properties can be imported into FDTD Materials Database manually. We can also define material properties through material database. “Sample data” and “Plasma (Drude model)” types are used to build material database in later simulations. When Hyperbolic Metamaterial is investigated, anisotropic sample data is imported computing by Effective Medium Theory. To further study how substrate properties would affect the light extraction efficiency, in section 4.2.7, plasma types is used to simulate perfect reflector.

2.3 Simulation Domain and Analysis Monitor

Needless to say, an Analysis domain is needed in FDTD simulation. FDTD solves Maxwell’s curl equations in non-magnetic materials within the simulation domain in every mesh unit.

$$\frac{\partial \vec{D}}{\partial t} = \nabla \times \vec{H} \quad (4)$$

$$\vec{D}(\omega) = \epsilon_0 \epsilon_r(\omega) \vec{E}(\omega) \quad (5)$$

$$\frac{\partial \vec{H}}{\partial t} = -\frac{1}{\mu_0} \nabla \times \vec{E} \quad (6)$$

where H, E, and D are the magnetic, electric, and displacement fields, respectively, while $\epsilon_r(\omega)$ is the complex relative dielectric constant $\epsilon_r(\omega) = n^2$, where n is the refractive index.

1) Create simulation Domain and Boundary Conditions



Click “Simulation” icon and create the simulation domain. Set the dimensions in “model--setup—script”. See Appendix A for setup code.

If periodic boundary conditions are used for the Domain, may lead to interference from neighboring dipoles. However, PML boundaries assume that fields absorbed by the boundaries and do not make it into the far field. So go to “FDTD-Edit object-Boundary conditions” to setup boundary conditions same as below. Noted that Z min boundary is located in the metal layer, so “metal” condition is used to define z min bc.

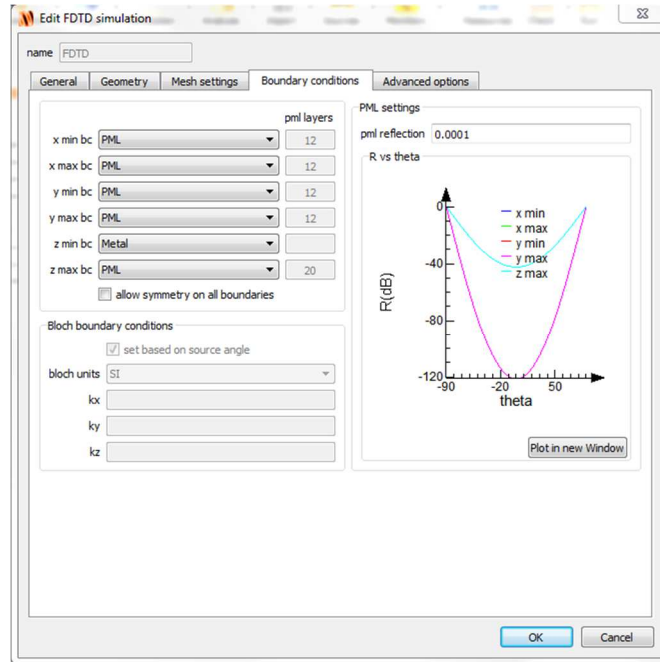


Figure 9: Boundary Conditions Setup Window

2) Add analysis groups

External Quantum Efficiency, which define as the ratio of extract photon to generate photon, could be calculate by far field power divided by dipole power in the simulation. Two variables, far field power and dipole power, are computed by two separate analysis groups. These two analysis groups own their monitors, Far field monitor and dipole power transmission box monitor, respectively. Fig.10 is the schematic of two monitors placed in the OLED device.

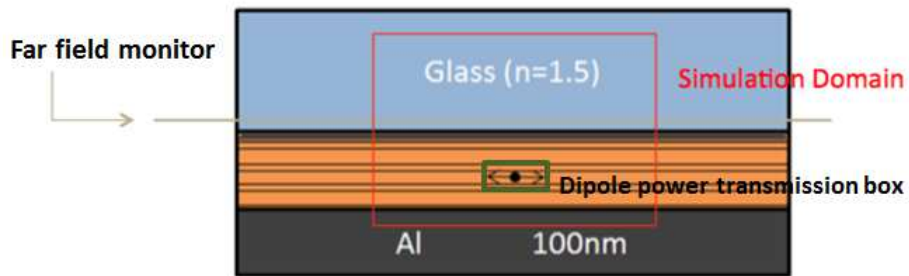


Figure 10: Schematic Numerical Model in FDTD

In addition, Fig.11 (a) and (b) below shows where to find these two types of analysis group in FDTD.

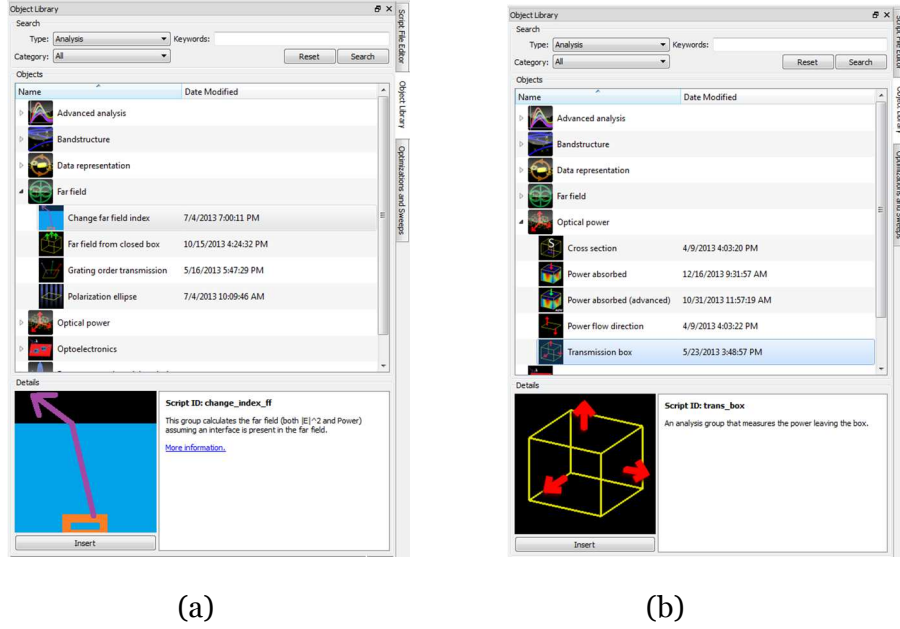


Figure 11: Analysis Group for (a) Far-field Emission and (b) Dipole Power Calculation

■ Far Field analysis:

Fraction of sourcepower transmitted to far field is derived from farfield analysis group. The monitor of the analysis group is placed inside of the glass layer in OLED structure, as it shows in Figure 10. The property of very far field refractive index is needed, in this case is $n=1$ for the air. The monitor returns the spherical complex electric fields to the analysis group, then calculate the hemispherical electric field and Power for both in glass (where monitor located) and into the air (very far field). The glass and air interface reaction is derived by Fresnel's Law.

$$(7) \quad \frac{1}{2} \sqrt{\frac{\epsilon_0}{\mu_0}} n_2 |E_2|^2 \cdot d\theta_2 d\psi_2 \sin \theta_2 = \frac{1}{2} \sqrt{\frac{\epsilon_0}{\mu_0}} n_1 \left(T_s \cdot |E_s|^2 + T_p \cdot |E_p|^2 \right) d\theta_1 d\psi_1 \sin \theta_1$$

where T_s and T_p calculated as below using Fresnel equations:

$$\rho_p = r_p^2 = \left(\frac{n_1 \cos \theta_2 - n_2 \cos \theta_1}{n_1 \cos \theta_2 + n_2 \cos \theta_1} \right)^2 \quad (8)$$

$$\rho_s = r_s^2 = \left(\frac{n_1 \cos \theta_1 - n_2 \cos \theta_2}{n_1 \cos \theta_1 + n_2 \cos \theta_2} \right)^2 \quad (9)$$

$$T_s = 1 - \rho_s \quad (10)$$

$$T_p = 1 - \rho_p \quad (11)$$

Since Snell's law proved that $\theta_2 = \sin^{-1} \left(\frac{n_1}{n_2} \right) \sin \theta_1$, and we have $d\theta_1 = d\theta_2$, we can simplify the equation to:

$$|E_2|^2 = \left(T_s \cdot |E_s|^2 + T_p \cdot |E_p|^2 \right) d\theta_1/d\theta_2 \quad (12)$$

All the dimension setups are included in “model -- edit object -- setup -- script” (Appendix A)

■ Dipole power analysis:

Use “transmission box”, an analysis group that measures the power leaving the box to achieve the dipole power emitted. The dimension of the box monitor should little bit larger than the dipole source projection, which is large enough not to miss any energy dipole project and small enough to avoid loss in emitting material.

Theoretical power radiated by an electric dipole in a homogeneous material is calculated by

$$P = \frac{\mu_0}{4\pi} n |\vec{p}_0|^2 \frac{\omega^4}{3c} \quad (13)$$

where p_0 (Cm) is the dipole moment and μ_0 is the magnetic permeability. Dipole Power in Non-homogeneous is calculated by Green's function and normalized to the analytic expression for the power radiated by this dipole in a homogeneous material.

Note: FDTD solutions can calculate dipole power by analytical method using Green's equation. However, analytical method does not work if the emitting layer's material is lossy ($k \neq 0$). Since the k value of emitting layer is negligible, we can use both monitor and analytical method in this case. In this simulation, box monitor method is applied.

See Appendix B and C for the script of two analysis group.

3) Programming logic related to the far field analysis script

Step 1. Determine the structure is 2D or 3D (3D in this case).

Step 2. Initialize variables with resolution of the far field.

Step 3. Get far field projection direction vectors and calculate the angle theta (with respect to z direction), which will be used in air-glass interface calculation.

Step 4. Get electric field and transmission power in the material that the monitor is located within.

Step 5. Calculate electric field and transmission power in far field using Fresnel coefficients, Snell's law, etc.

2.4 Meshing

Right click "FDTD" in the objects tree, and select Edit object, click mesh settings. In general cases, automatic mesh can be applied. However, in this case, the thicknesses of layers in OLED are too small, custom non-uniform mesh type is used instead to finer the mesh along z direction. Maximum mesh step settings applied as below:

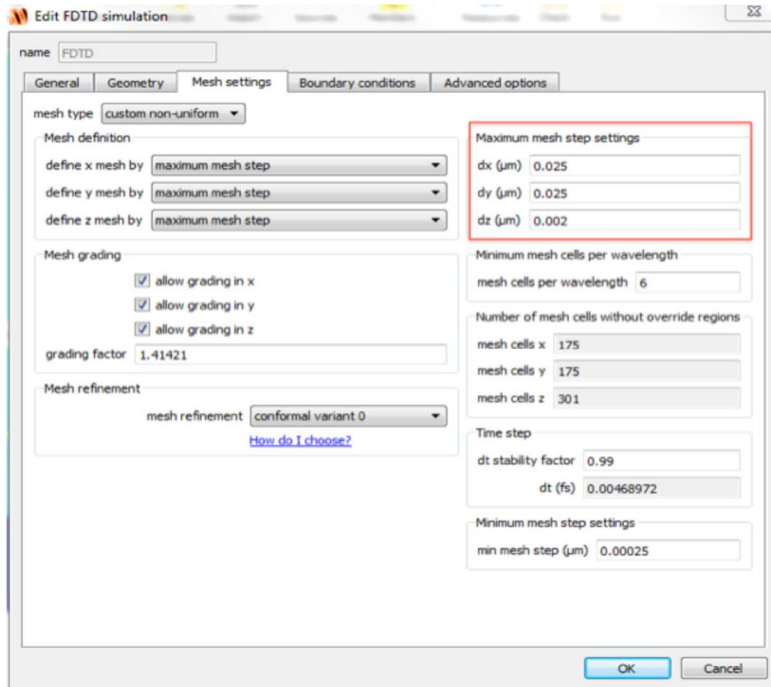



Figure 12: Mesh Setting Window For the Whole Domain

For dipole source box monitor, a finer override mesh is needed. Open the menu

of  and select “mesh”. Position and geometry is set in the model setup script (Appendix A). To define the mesh size, right click the “mesh” in objects tree, and select Edit object. Then define as below:

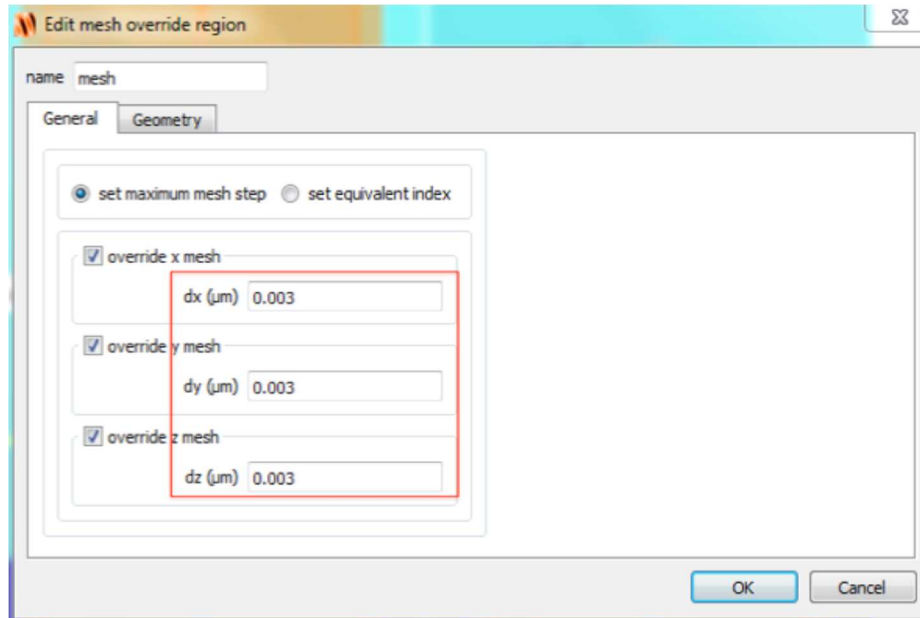


Figure 13: Edit Window For Override Mesh

2.5 Convergence Check

After all the set ups, to make sure the accurate simulation can be achieved, convergence check is unneglectable. Major convergence factors that ensure the numerical accuracy in FDTD simulations for OLEDs are list below.

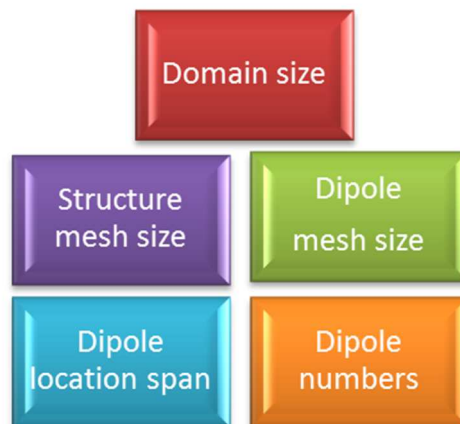


Figure 14: Major Convergence Factors that Ensures the Numerical Accuracy in FDTD Simulations for OLEDs

In order to do the convergence check for every factor, the method is fixing other factors and changing the factor that you want to investigate one at a time. Take “Domain size” as an example, fix all other factors and only change the domain size, from smaller size to bigger size. Plot the “Extraction efficiency” from all domain size to see whether the change of domain size resulting in a big varies of the Extraction efficiency. If the error is small enough, the results is considered converging under that arbitrary domain size. Repeat the same convergence check for all the factors to get valid simulation result.

2.6 Sweep Tool

Because dipoles are spontaneously emitting in the active layer of an OLED, sweep tool should be set up to average the results from multiple simulations. Multiple simulations include three orientations under different locations on z direction. Since the structure used in this thesis are all isotropic in x-y direction, only horizontal direction need to be considered. Write script file to calculate average result of multiple simulations for different dipole orientations and positions. Right click “pattern_dipole_position” and select Edit object. Enter Number of points, location range and orientation as below:

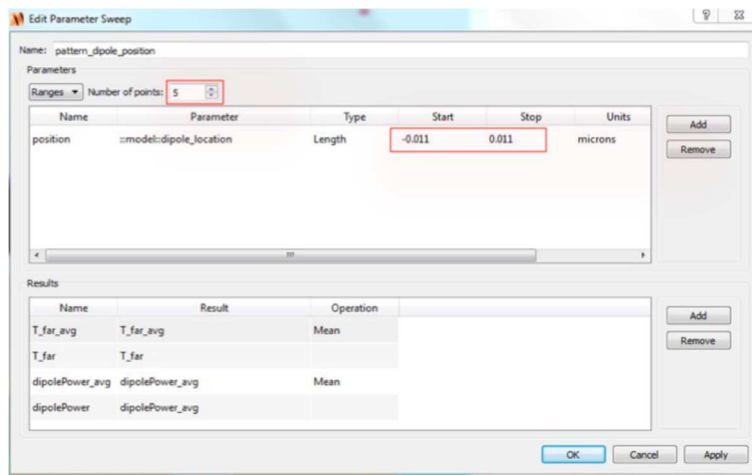


Figure 15: Setup Dipole Location and Numbers in Sweep Tool

Script for the sweep file is attached on appendix D, which is applied to calculate the Extraction Efficiency ($\frac{\text{Far Field Power}}{\text{Dipole Source Power}}$) in each simulation and get the average result of those results.

Chapter 3

PHOTONIC CRYSTAL STRUCTURE

3.1 Introduction

Photonic Crystal Structure consists of alternating dielectric layers located between ITO and glass substrate. This kind of structure has properties that can manipulate photons, in much the same way as the semiconductors manipulate electrons. Photonic crystals usually contain periodic multilayers with unit cell of two dielectric layers with high and low relative permittivity. It allows certain wavelengths of electromagnetic wave to propagate through the structure, while block some of the wavelengths. Wavelengths that are disallowed to pass the structure are called band gaps, or stop bands. This photonic crystal is also known as Distributed Bragg Reflector (DBR) in optical field. Because light within the wavelengths of stop bands is forbidden to propagate, these light will be highly reflected back by the structure. Thus, DBR can be used as a high-quality reflector in OLED. Together with cathode, DBR pairing structure can create resonance and lead to the enhancement of the light extraction efficiency. Ecton proposed a micro cavity OLED by using DBR pairs in his PhD dissertation. In this chapter, his structure is reproduced by FDTD solutions. Schematic of the structure is showed below.

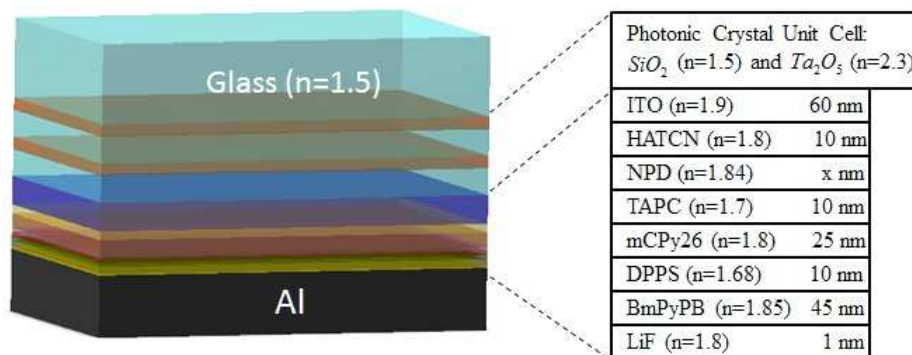


Figure 16: Schematic of Photonic Crystal Structure OLED

Between the ITO layer and glass layer, locates the photonic crystal structure, which is periodic layers with unit cell of SiO_2 and Ta_2O_5 . One-pair structure, from upper to lower layer, consists of Glass, Ta_2O_5 (57 nm), SiO_2 (100 nm), ITO. Two-pair structure contents Glass, Ta_2O_5 (57 nm), SiO_2 (83 nm), Ta_2O_5 (57 nm), SiO_2 (100 nm), ITO. And three-pair are Ta_2O_5 (57 nm), SiO_2 (83 nm), Ta_2O_5 (57 nm), SiO_2 (83 nm), Ta_2O_5 (57 nm), SiO_2 (100 nm). Applied photonic crystal under glass substrate is aiming to minimize the organic mode in OLED device.

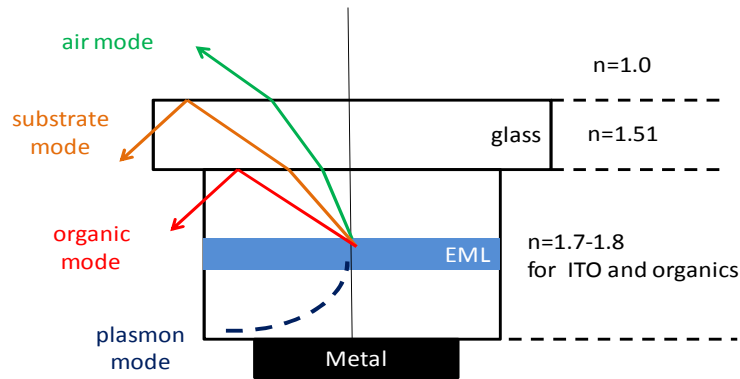


Figure 17: Mechanism of Losses in OLED Structure

As it shows in Figure 17, some of the light trapped in the organic layers due to the total internal reflectance. Periodic of dielectric layers create a reflector using its stopband and formed a cavity structure inside the device. The structures are expected to enhance the light extraction efficiency by interference effect.

3.2 Results and Discussion

Figure 18 below is the results of photonic crystal structure OLED under following setups: Domain size 4 μ m, Dipole Box Monitor size: 20nm, Dipole mesh size 2nm*2nm*3nm. Structure mesh size: 25nm*25nm*2nm. Dipole sweep: Z span \pm 11nm, 5 simulations with 3 orientations each.

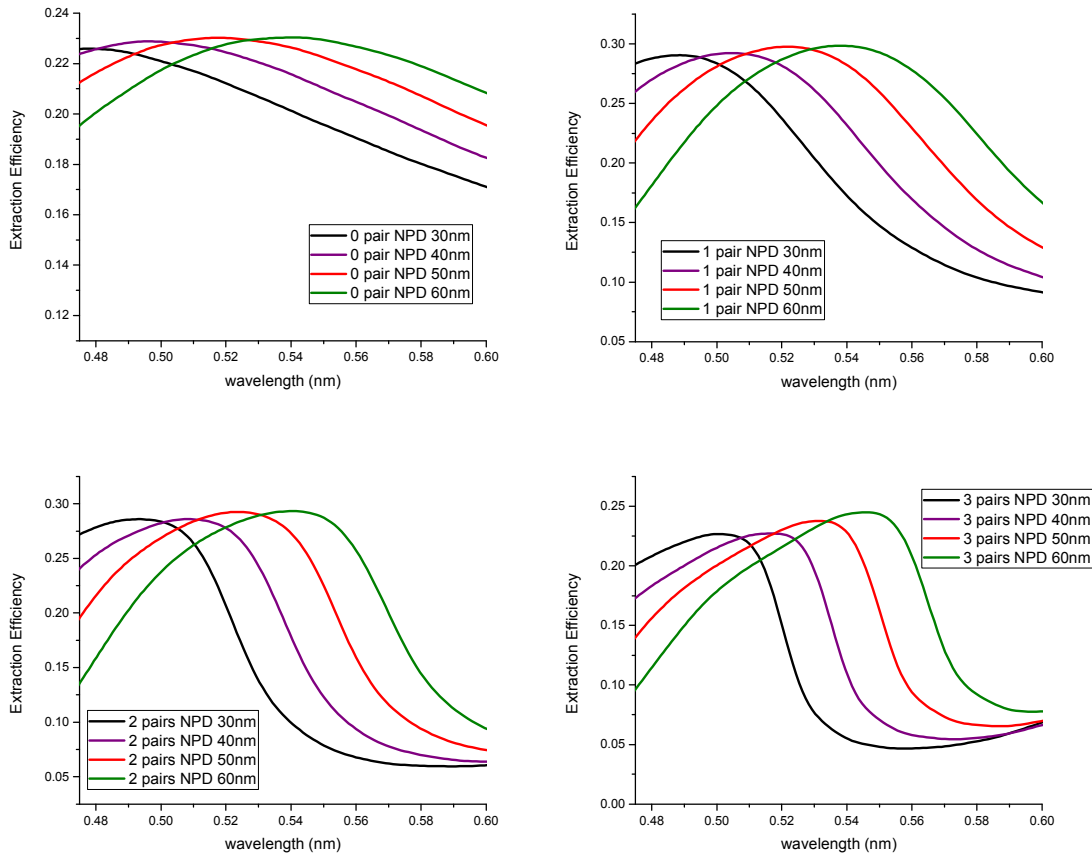


Figure 18: Results of Photonic Crystal Structures

As indicated by Figure 18, the extraction efficiency for the photonic crystal structures increases comparing to 0 pair conventional OLED structures. It is observed that the maximum efficiencies are 23%, 30%, 30% and 25% for 0 pair, 1 pair, 2 pairs and 3 pairs, respectively. 0 pair conventional device has a broad band wavelength of extraction. In contrast, structures with more pairs have relatively narrow band of out-

coupling. This is due to the bandgap which photonic crystal structure creates. If two mirrors causing resonance with interference effect, certain wavelengths will be reinforced, while other wavelengths will be blocked inside the structure. The band gap effect becomes obvious with the increasing of pair numbers. It is shown that 1 pair and 2 pairs photonic crystal structure own better results compare to the other proposed structures.

On the other hand, changing the thickness of NPD layer could tune the emission peak of the device. It is noticed that the emission band red shifts to longer wavelength as the NPD layer gets thicker. This is because the resonance wavelength is proportional to the cavity thickness. Note that optimum efficiencies occurs at the almost the same wavelength with same thickness of NPD layer, no matter how many pairs there are in the photonic crystal structure. Furthermore, Interference effect is proved to be the physical mechanism of this photonic crystal structure by using analytical method in chapter 5.

3.3 Effect of Dispersive Optical Constants of Materials

Constant refractive index and zero extinction coefficients are used to reproduce Jeremy's structure in section 3.2. Additionally, simulation using wavelength dependent refractive index and extinction coefficient is utilized to further study how to simulate realistic problem. Meanwhile, geometry setups remain the same. Figure 19 below shows the comparison results from fixed refractive indices and dispersive ones. Some of the

materials used in the structure have relatively high extinction coefficient near 400nm wavelength. NPD as an example, the extinction coefficient is around 0.15 when 400nm wavelength. Thus, the extraction efficiencies near 400nm wavelength are less than the previous results when consider k as zero. For more material properties, see Appendix A.

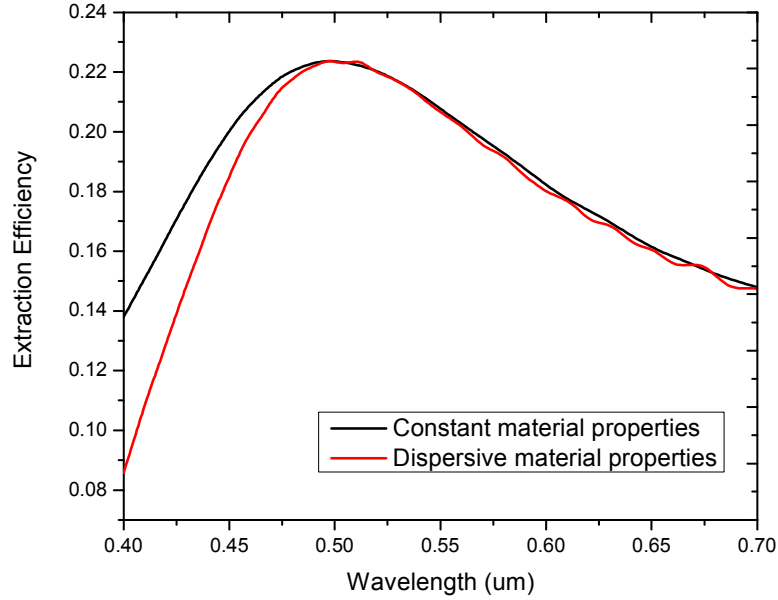


Figure 19: Comparison Between Two Simulation Results Under Zero DBR Pair and NPD Thickness 40nm.

Chapter 4

FABRY-PEROT RESONANCE CAVITIES

4.1 Simulation Setup

Fabry-Perot cavity resonance is usually made of a transparent plate sandwiched between two reflecting surfaces, or two parallel highly reflecting mirrors. This structure will cause light interference between two mirrors and thus enhance the light at some specific wavelength. In OLED structure, anode and cathode are needed, and materials between them are all transparent with k approximately equal to zero. In this chapter, both anode and cathode are designed as reflecting mirrors to make OLED structure a Fabry-Perot cavity, thus enhanced the extraction efficiency at a specific wavelength. Since the anode of the device would be thin enough to allow visible light pass, Light Extract Efficiency is worth investigating under this fact. Figure 20 shows the revised Fabry-Perot structure. This following chapter shows how Fabry-Perot cavity resonance will affect OLED Light Extraction Efficiency. Substrate Al (Cathode) and 60nm Metal (Anode) layer are the two mirrors in Fabry-Perot cavity.

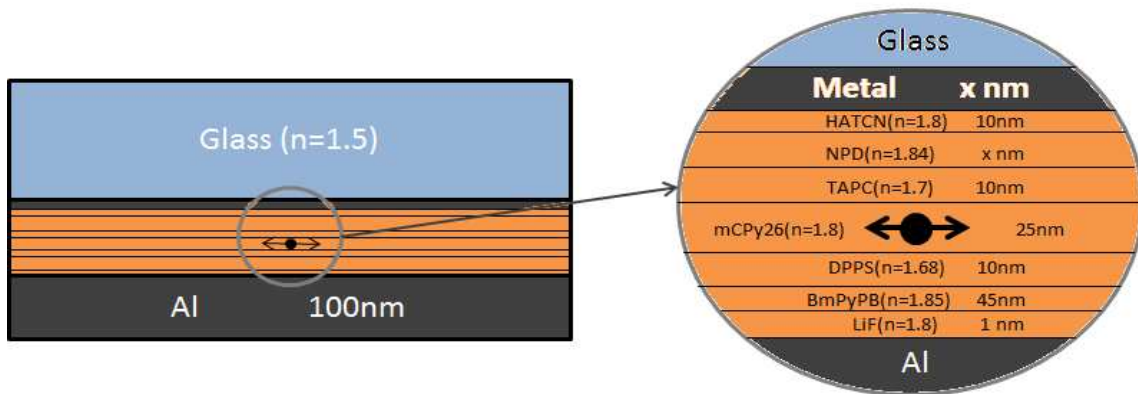


Figure 20: Proposed Fabry-Perot Cavity OLED

In this proposed structure, compare to the DBR Pairing structure, only anode layer's material is changed. Since results for Photonic crystal structure are converged in chapter 3, same setup is chosen:

Setup: Domain size 4 μ m, Dipole Box Monitor size 20nm, Dipole mesh size 2nm \times 2nm \times 3nm. Structure mesh size 25nm \times 25nm \times 2nm.

Dipole sweep: Z span \pm 11nm, 5 simulations with 3 orientations each.

4.2. Factors That Affect Spectrum Extraction

4.2.1. Different Materials for Anode Layer

Three materials: Aluminum (Al), Silver (Ag) and Gold (Au) for anode layer are investigated in Fabry-Perot Cavity OLED. Parameters and results are indicated in Table 2.

Case	Material	Thickness (d)	Maximum extraction efficiency
1	Aluminum (Al)	10 nm	20%
2	Gold (Au)	10 nm	27.5%
3	Silver (Ag)	10 nm	30.5%

Table 2: Different Materials of Metal Layer and Corresponding Simulation Results

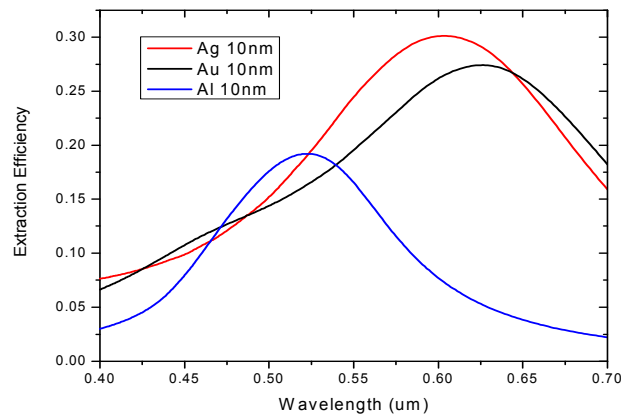


Figure 21: Spectrum Extraction Efficiency of Different Cases Above (table 2)

As is shown in the result, when using silver as anode, extraction efficiency peak is around 0.6um and the value is around 0.3. Gold anode structure, however, is less efficient than silver one. Efficiency peak for gold anode structure is 0.275 at 0.625um. Aluminum has the worst efficiency, 0.2, comparing to others. The failure of using Aluminum is because its high extinction coefficient in visible range. Therefore, silver (Ag) and gold (Au) are relatively better choices for Fabry-Perot OLED structure.

4.2.2. Thickness of the Anode Layer

Thickness of the metal layer also has remarkable influence on the Light Extraction Efficiency, this factor is further investigated by simulations with different metal layer thicknesses (Table 3).

Case	Material	Thickness (d)	Maximum extraction efficiency
1	Silver (Ag)	5 nm	27%
2	Silver (Ag)	10 nm	30.5%
3	Silver (Ag)	15 nm	31%
4	Silver (Ag)	18 nm	34%
5	Silver (Ag)	20 nm	34%
6	Silver (Ag)	22 nm	34%
7	Silver (Ag)	25 nm	30%

Table 3. Different Thicknesses of Silver Layer and Corresponding Simulation Results

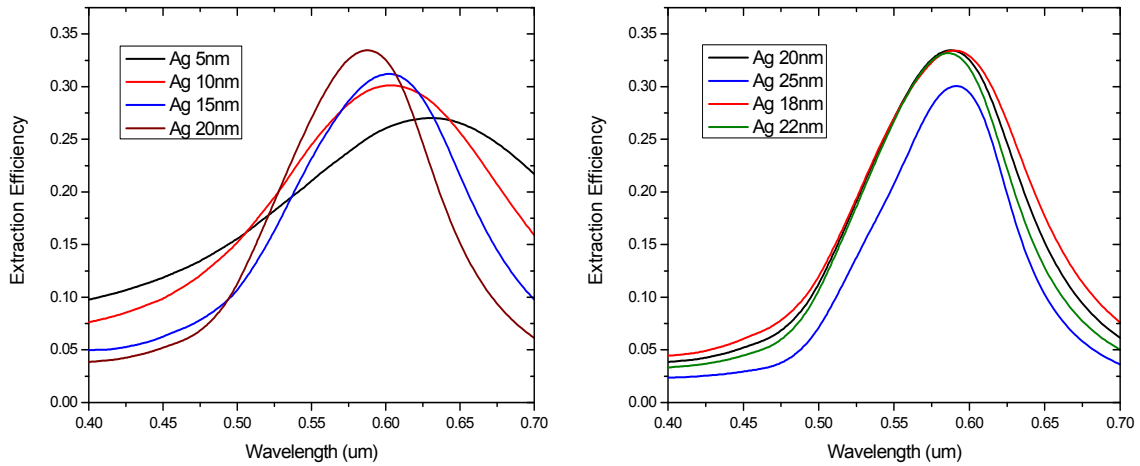


Figure 22: Spectrum Extraction Efficiency of Different Cases Above (table 3)

It is obvious when thickness is less than 20nm, the extraction efficiency increases as the metal layer gets thicker. It will reach optimum value at around 18nm and start decreasing after. In addition, maximum value blue shifts as metal layer becomes thicker.

Furthermore, it is essential to know whether the efficiency of gold anode structure will exceed the silver anode structure efficiency by changing the thickness of gold (Au) layer.

Case	Material	Thickness (d)	Maximum extraction efficiency
1	Gold (Au)	5 nm	26.5%
2	Gold (Au)	10 nm	27.5%
3	Gold (Au)	15 nm	25%

Table 4: Different Thicknesses of Gold Layer and Corresponding Simulation Results

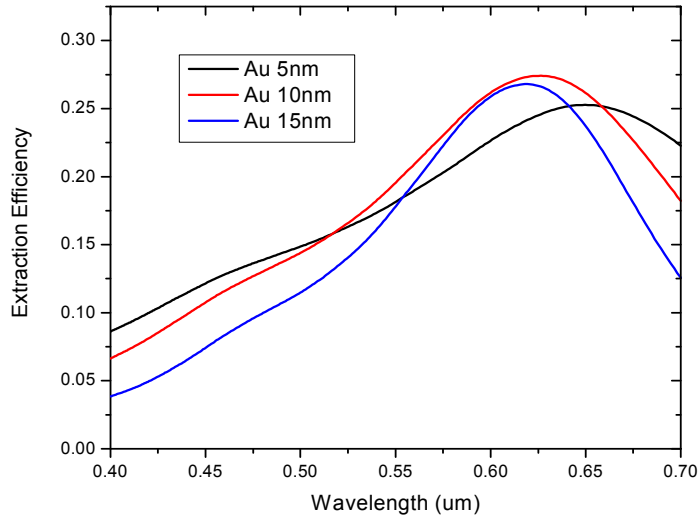
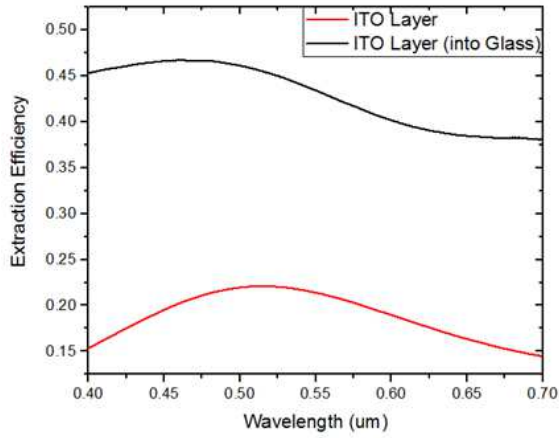


Figure 23: Spectrum Extraction Efficiency of Different Cases Above (table 4)

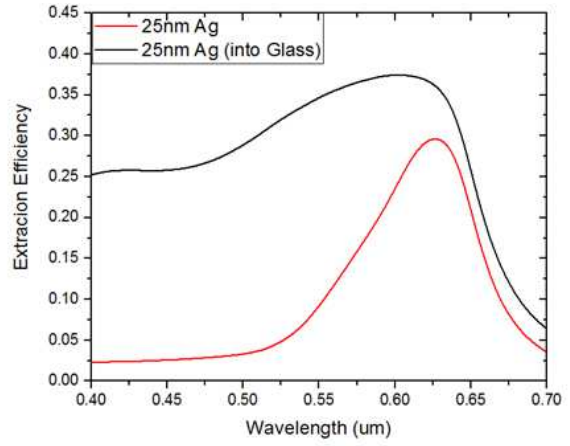
As is indicated in Figure 23, the peak value occurs around 10nm thickness and will drop whenever it goes thinner or thicker. As a result, silver is better than gold for anode in the Fabry-Perot OLED structure.

4.2.3 Field concentration effect

It is worth noting that Fabry-Perot Structure can only enhance the extraction efficiency in a relatively narrow wavelength range. This narrow wavelength range optimized by the structure could be used to tune the color for white source OLED. Comparison is made with the conventional structure which consists of ITO Layer as anode. Original ITO structure of OLED has higher light extraction efficiency into the glass layer, but less out-coupling light into the air. The difference is because the total internal reflectance happened on glass-air interface. Fabry-Perot structure focus the dipole radiation within a small angle, thus increases out-coupling efficiency on the glass-air interface according to Fresnel's Law of Reflectance. The plot below shows a strong focusing effect of Fabry-Perot structure at 639nm wavelength.

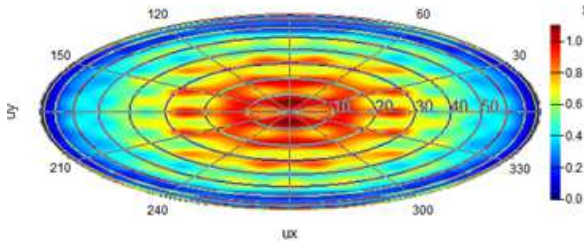


(a)

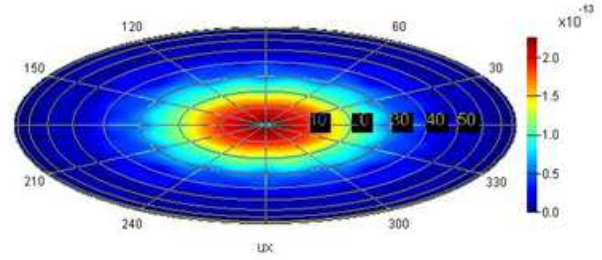


(b)

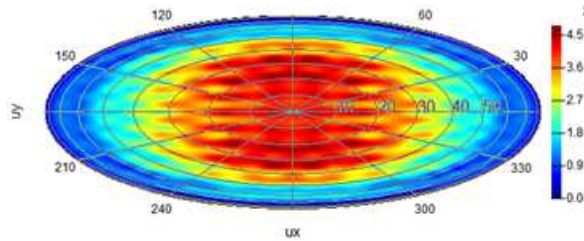
E field into glass at 639nm (ITO)



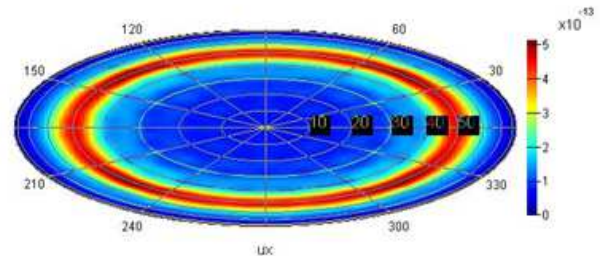
E field into glass at 639nm (Fabry-Perot)



E field into glass at 476nm (ITO)



E field into glass at 476nm (Fabry-Perot)



(c)

Figure 24: Comparison of ITO Structure with Fabry-Perot Structure Device (a) Extraction Efficiency of ITO structure (b) Extraction Efficiency of Fabry-Perot structure (c) Electric Field of Different Structure at Different Wavelength

Figure 24 (c) shows the Electric Field of Fabry-Perot structure at 476nm wavelength. Instead of concentrating the electric field within a small range, the structure

diffracts the light to larger angle in order to obtain the low extraction at other wavelength, thus achieve the optical selectivity.

4.2.4. Thickness of NPD Layer

In DBR structure (chapter 2), the thickness of NPD layer affects the emission peak of light extraction efficiency. When using Fabry-Perot cavity in OLED, thickness of NPD layer would change the cavity thickness and affect the results as well. Optimum output wavelengths range can be adjusted by altering NPD thickness. The distance between two mirrors can affect the wavelength of interference. The out-coupling efficiency reaches maximum value when total internal reflectance is minimized. That is to say, when the EM wave reflected from bottom mirror canceled what reflected from upper mirror by interference, optimum output efficiency can be derived. Cancellation of EM wave can be obtained by phase shift of π . According to the phase shift in the case of

plan wave source ($\beta = \frac{2\pi n_c d_c \cos \theta_c}{\lambda}$ (14), where n_c represents index of the cavity, d_c is

the thickness of cavity and θ_c is the incident angle.) , optimum wavelength should be proportional to the cavity thickness. Thus, when the thickness of NPD layer becomes larger, the out-coupling efficiency red shifts accordingly.

Case	Thickness of NPD Layer	Maximum extraction efficiency
1	15 nm	540 nm
2	20 nm	560 nm
3	25 nm	580 nm
3	30 nm	600 nm

Table 5: Varies Thicknesses of NPD Layer and Corresponding Simulation Results

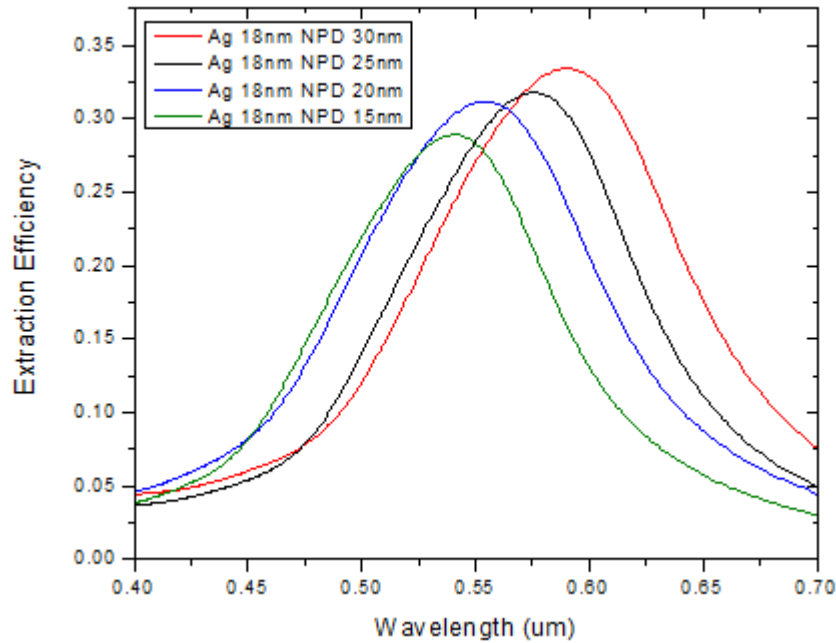


Figure 25: Spectrum Extraction Efficiency of Different Cases Above (Table 5)

4.2.5 Dipole Polarizations and Locations

Results above are all derived by sweep tool in FDTD (section 2.1.5). Sweep tool is utilized to average the results of different dipole locations and polarizations. The following section reveals how dipole location and polarization affects the external quantum efficiency. Different dipole location is simulated to investigate whether the location of dipoles will largely affect the result. The thickness of organic emitting layer is 25nm. Upper dipole, which is located 7nm higher than the center of emitting layer, is slightly more efficient than dipoles below. However, the influence is relatively insignificant.

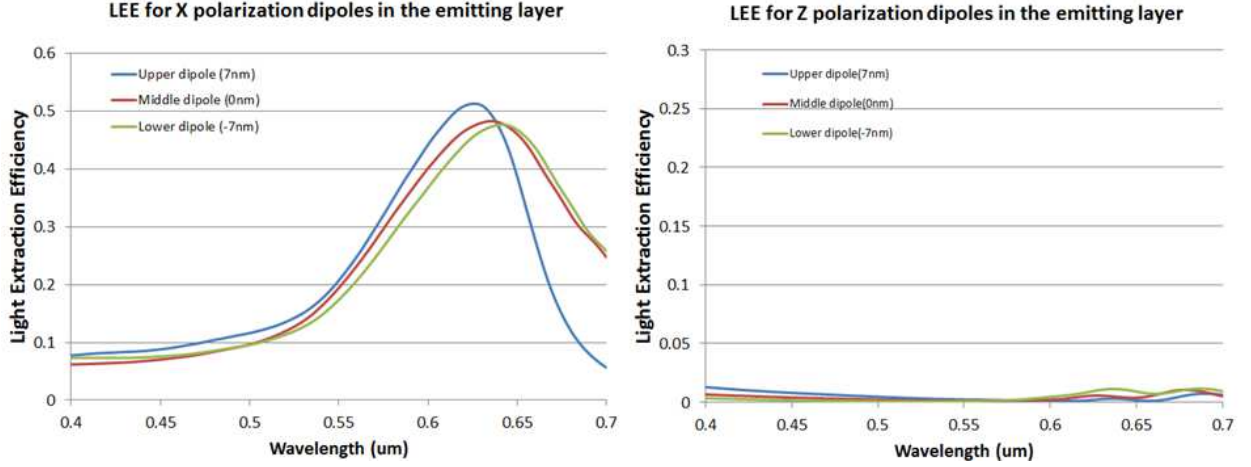


Figure 26: Light Extraction Efficiency of a Single Dipole at Different Conditions

Dipole orientation plays an important role on the out coupling efficiency. This multilayer structure is isotropic in x and y direction. X and Z polarization dipoles are simulated accordingly. As is shows in figure 26, dipoles of x polarization have much larger external quantum efficiency than dipoles of z polarization. Therefore, an OLED with Fabry-Perot structure can reach 50% of EQE if only x polarization dipoles are emitted by the organic layer. According to the simulation above, engineering a single dipole polarized OLED is a huge potential for efficiency improvement.

4.2.6 Ray Tracing Method

Defaults calculation from far field analysis group in FDTD considers only single transmission. However, in real life cases, multiple reflection and transmission would happen on every interface. Considering multiple reflection and transmission, ray tracing method is chosen to simulate the light extraction efficiency. According to the schematic below, total transmittance of glass to the air is calculated by

$$T_2 = t_2 + t_2 r_2 r_1 + t_2 r_2^2 r_1^2 + t_2 r_2^3 r_1^3 + t_2 r_2^4 r_1^4 + \dots = \frac{t_2}{1 - r_2 r_1} \quad (15), \quad \text{where } t_1 \text{ represents}$$

transmittance from glass to OLED structure. t_2 is the transmittance at glass/air

interface. r_1 and r_2 are the reflectance at these two interfaces. Field Monitor in FDTD gives the value of electromagnetic field in glass layer without considering any interaction from air/glass interface. Total transmittance T_2 is the coefficient multiplied to derive the total transmitted EM field into the air. r_1, r_2 and t_2 can be numerically calculated by FDTD solution following Fresnel's Law, thus T_2 can be derived.

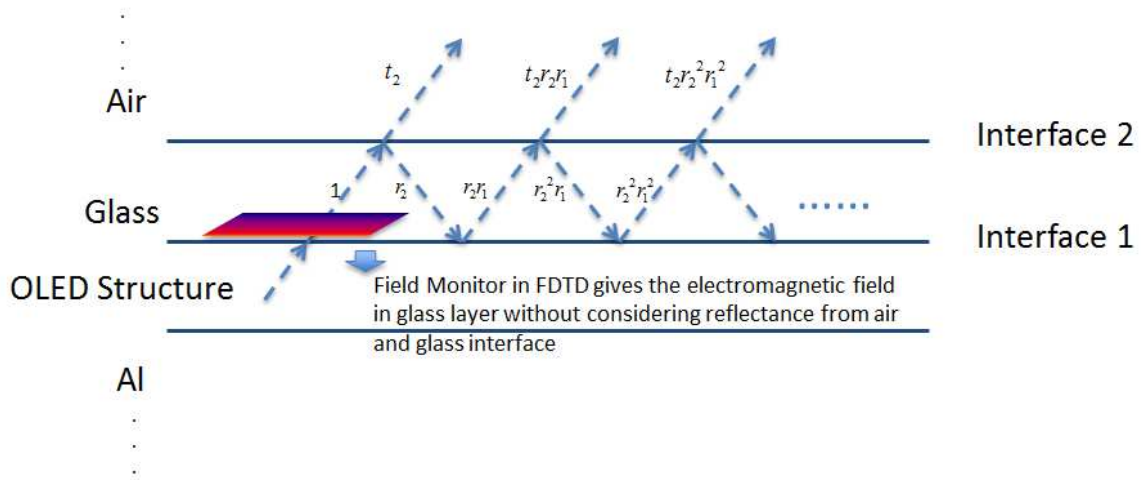


Figure 27: Schematic of the Ray Tracing Method Calculation

Figure 28 below shows the comparison results for ray tracing method and single transmission method. Result with ray tracing method gives 2% of increase, which made the simulation more accurate.

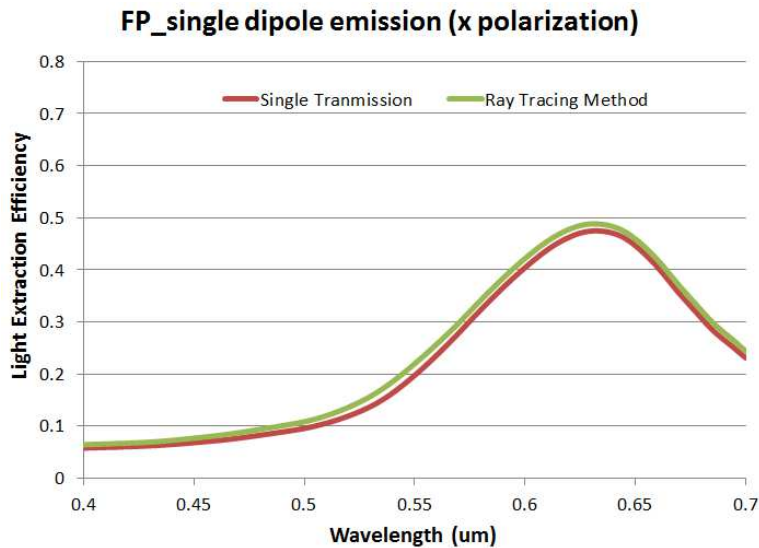


Figure 28: Comparison Results of Single Dipole With and Without Ray-Tracing Method

4.2.7 Perfect Reflector as Cathode

Non-absorb cathode is applied to eliminate the absorption energy loss in OLED structure. It is worth to point out that all layers except for medal layers in OLED device are already simulated using non-absorb properties ($k=0$). Perfect reflector does not exist in real world. However, simulate cathode as perfect reflector can gives the upper limit for maximum extraction efficiency. Drude model is clarified as below to introduce the concept of perfect reflector.

Drude model considers that conductive materials consist of free electrons move randomly inside of the structure. After applying an electromagnetic field, free electrons start to move under average velocity. Thus, the EM field gives rise to electric current oscillating at the same frequency. Because the immobile atoms inside the material will prevent free electrons from moving, a damping force will occur on the electrons. The motion equation of a free electron is

$$m_e \ddot{x} = -m_e \gamma \dot{x} - eE \quad (16)$$

m_e in the equation is the electron mass, e is the charge of the electron, and γ represents the damping factor due to the collision with immobile atoms. Assume that a harmonic field $E = E_0 e^{-i\omega t}$ will result the electron move as $x = x_0 e^{-i\omega t}$, thus $\ddot{x} = -i\omega \dot{x}$.

Substitute into previous equation to get

$$\dot{x} = \frac{e/m_e}{i\omega - \gamma} E \quad (17)$$

Electric current density is defined as $J = -n_e e \dot{x} = \tilde{\sigma}(\omega) E$. So the complex conductivity can be expressed by

$$\tilde{\sigma}(\omega) = \frac{n_e e^2 / m_e}{\gamma - i\omega} = \frac{\sigma_0}{1 - i\omega / \gamma} \quad (18)$$

where σ_0 is the dc conductivity equals to $n_e e^2 \tau / m_e$. Furthermore, relationship between dielectric function and the conductivity can be built as following equation:

$$\varepsilon(\omega) = \varepsilon_\infty - \frac{\sigma_0 \gamma}{\varepsilon_0 (\omega^2 + i\gamma\omega)} \quad (19)$$

ε_∞ here denotes the contributions that are crucial at high frequencies, which is approximately equals to 1. Additionally, Plasma frequency is introduced based on $\omega_p^2 = \sigma_0 \gamma / \varepsilon_0 = n_e e^2 / m_e \varepsilon_0$. Thus, in Drude model, frequency-dependent dielectric function of a metallic material can be written as

$$\varepsilon(\omega) = \varepsilon_\infty - \frac{\omega_p^2}{\omega(\omega + i\gamma)} \quad (20)$$

Cathode in this Fabry-Perot structure OLED is Aluminum, which ω_p equals to $2.4 \times 10^{16} \text{ (rad / s)}$ and damping factor γ equals to $1.4 \times 10^{14} \text{ (rad / s)}$ using Drude model. To simulate cathode as perfect reflector, no loss is considered in this material, therefore the damping factor equals to 0 instead of $1.4 \times 10^{14} \text{ (rad / s)}$.

Material properties are set using “plasma type” in FDTD. Two variables, plasma frequency and damping factor, are needed. $2.4 \times 10^{16} \text{ (rad / s)}$ for ω_p and $1.4 \times 10^{14} \text{ (rad / s)}$ for γ when simulating Drude model Al. $2.4 \times 10^{16} \text{ (rad / s)}$ for ω_p and 0 for γ when simulating Al as perfect reflector.

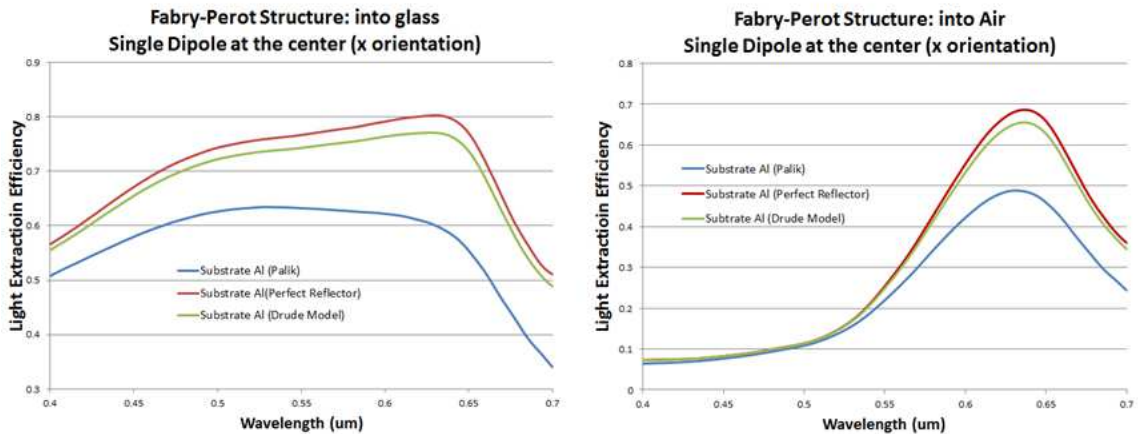


Figure 29: Light Extraction Efficiency of Fabry-Perot Structure Simulated using Palik Data, Drude Model and Perfect Reflector Model for Al layer

Figure 29 shows the light extraction efficiency of single dipole at the center of emitting layer. When simulate An efficiency of 70% is reached when considering Al as perfect reflector. In contrast, using Palik data for Al only gives 49% of the extraction efficiency. On the other hand, Drude model simulation gives a relatively high performance as 65% external quantum efficiency. Note that Palik data gives the material properties most close to the reality. However, perfect reflector Al as cathode indicates the upper limit efficiency of OLED could get. It is theoretically predicted that with the glass layer modification and Al material improvement, a maximum of 80% light extraction efficiency could derived. In conclusion, applying advanced, low loss Al as cathode could eliminate the absorption loss in Organic LEDs.

Chapter 5

ELUCIDATING PHYSICAL MECHANISM WITH ANALYTICAL MODEL

Since the light source of OLED is inside the structure, the physical mechanism is hard to elucidate directly by analytical model. Instead, if a relationship can be built between the reflectance of the structure and the light extraction efficiency of the Organic LEDs, it would not only help explaining the physical mechanism but also facilitating future design. Assume the enhancement by photonic crystal structure and Fabry-Perot structure is due to the interference effect. Thus, the reflection dip for the structure must be on the same wavelength of the optimum extraction efficiency for this OLED. Because the extraction efficiency is derived within the whole hemisphere above the device, the reflectance, correspondingly, is referred to the spectral hemispherical-hemispherical reflectance \widehat{R}_λ .

$$\widehat{R}_\lambda(\lambda) = 2 \int_0^{\pi/2} R'_\lambda(\lambda, \theta) \cos \theta \sin \theta d\theta \quad (21)$$

where $R'_\lambda(\lambda, \theta)$ is the directional-hemispherical reflectance that can be derived by Transfer Matrix Method. The relationship between $\widehat{R}_\lambda(\lambda)$ and the light extraction efficiency will be investigated in this chapter. The physical mechanism can be further proved afterwards.

5.1. Transfer Matrix Method

Transfer Matrix Method is used to analysis the electromagnetic waves propagation inside a multilayer medium. Transfer matrix method was derived based on Maxwell's equations where a simple continuity conditions for the electric field across the boundaries from one medium to another medium. This method will then be used to derive the directional-hemispherical reflectance of multilayer structure of OLED. If a TE

wave, which angular frequency is ω , propagating in j th layer, the Electric field can be written as

$$E_j = E_{y,j} \hat{y} = E_j(z) e^{i(\beta x - \omega t)} \hat{y} \quad (22)$$

Assuming A_j and B_j represent the amplitudes of forward and backward waves in j th layer, electric field in each layer can be derived as

$$E_1(z) = A_1 e^{ik_{z1}z} + B_1 e^{-ik_{z1}z}$$

$$E_j(z) = A_j e^{ik_{zj}(z-z_{j-1})} + B_j e^{-ik_{zj}(z-z_{j-1})} \quad (j=2,3,4,\dots,N) \quad (23)$$

where z_j is the total thickness of j layers, $z_j = z_{j-1} + d_j$. Then, the magnetic field can be calculated by the Maxwell equation. Thus, the z -component Poynting vectors can be written as

$$S_{1z} = \frac{k_{z1}}{2\omega\mu_0} (A_1 A_1^* - B_1 B_1^*)$$

$$S_{jz} = \frac{1}{2} \text{Re} \left[\frac{k_{zj}^*}{\omega\mu_0\mu_j} (\psi_1 - \psi_2 - \psi_3) \right] \quad (24)$$

where $\psi_1 = |A_j|^2 e^{2\text{Re}(ik_{zj})(z-z_{j-1})}$, $\psi_2 = |B_j|^2 e^{-2\text{Re}(ik_{zj})(z-z_{j-1})}$ and $\psi_3 = 2i \text{Im} \left[A_j B_j^* e^{i2\text{Im}(ik_{zj})(z-z_{j-1})} \right]$

(25). After taking the boundary conditions into account, the relationship between adjacent layers can be expressed by

$$\begin{pmatrix} A_j \\ B_j \end{pmatrix} = P_j D_j^{-1} D_{j+1} \begin{pmatrix} A_{j+1} \\ B_{j+1} \end{pmatrix} \quad (26)$$

where, P_j is the propagation matrix and D_j is the dynamical matrix and given by

$$P_j = \begin{bmatrix} 1 & 0 \\ 0 & 1 \end{bmatrix}, \text{ when } j=1$$

$$P_j = \begin{bmatrix} e^{-ik_{zj}d_j} & 0 \\ 0 & e^{ik_{zj}d_j} \end{bmatrix}, j=2,3,\dots,N-1$$

$$D_j = \begin{bmatrix} 1 & 1 \\ \frac{k_{zj}}{\mu_j} & -\frac{k_{zj}}{\mu_j} \end{bmatrix}, j=1,2,3,\dots,N-1 \quad (27)$$

Hence, transmission and reflection coefficients can be attained by

$$\begin{pmatrix} A_1 \\ B_1 \end{pmatrix} = M \begin{pmatrix} A_N \\ B_N = 0 \end{pmatrix}, \text{ where } M = \prod_{l=1}^{N-1} P_l D_l^{-1} D_{l+1}$$

$$r = \frac{B_1}{A_1} = \frac{M_{21}}{M_{11}} \quad (28)$$

The spectral directional-hemispherical reflectance of a multilayer structure can then be calculated by

$$R'_\omega = rr^* = \left| \frac{M_{21}}{M_{11}} \right|^2 \quad (29)$$

5.2. Comparison between Analytical Model and Numerical Model

Figure 30 shows reflectance and light extraction efficiency of several Fabry-Perot structures. Parameters are shown on the titles of each plot. It can be noticed that the reflection dip for every OLED structure is at the same wavelength of optimum light extraction efficiency.

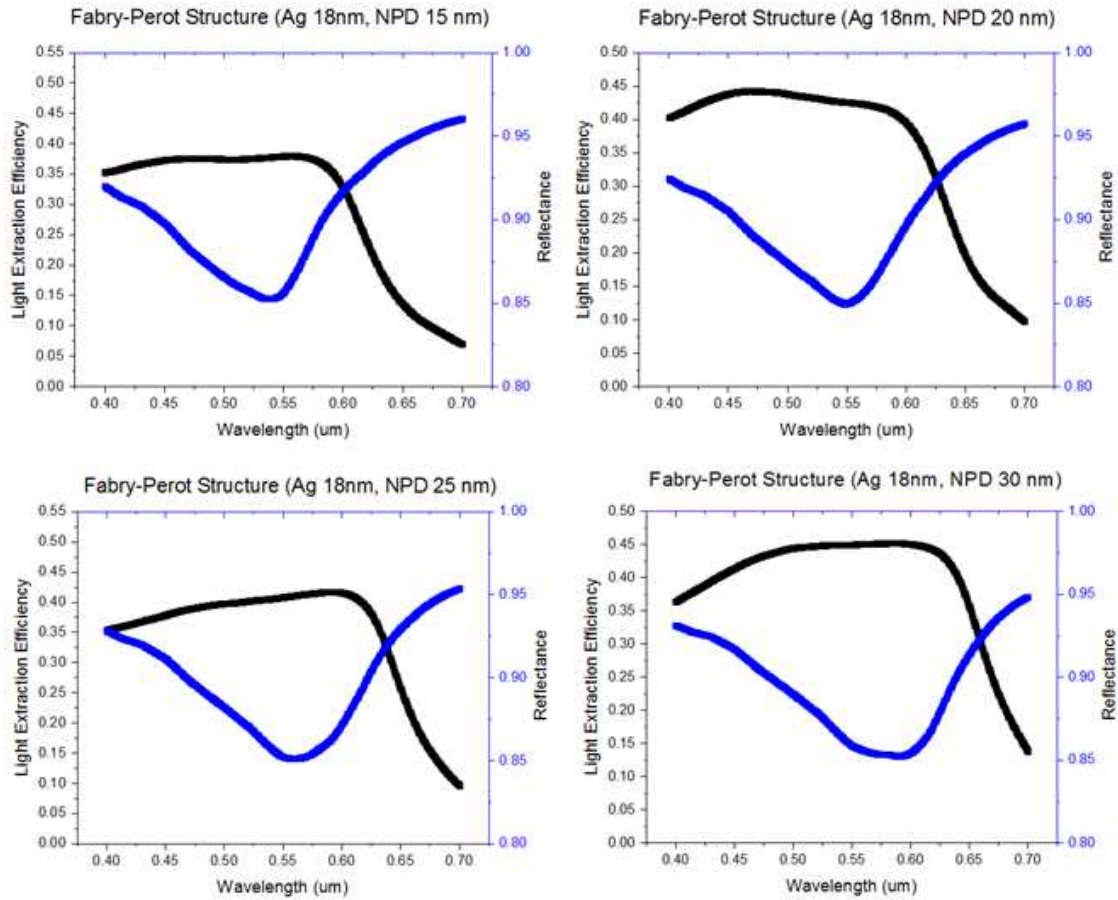


Figure 30: Comparison Between the Light Extraction Efficiency and Reflectance

In Figure 30, Fabry-Perot Structure with 30nm NPD layer has the reflection dip around 580nm. The Light Extraction Efficiency (LEE) peak locates on the same wavelength approximately. The reflectance would blue shift when applying smaller thickness of NPD layer. Correspondingly, the external quantum efficiency curve changes the same way as the reflectance curve. Moreover, as the plots indicated, not only the peak and dip located on the same wavelength, but also the shapes of these curves are similar inversely. Same trend can be observed in every case. The reflectance dip is due to the energy confinement inside of the structure. This reinforce of energy inside lead to a high absorption of the structure. Another way to explain this phenomenon is, according to the

Kirchhoff's law, if the structure can absorb large amount of energy, it can emit a large amount of energy in this spectral as well.

Low reflectance of the structure indicates the interference effect happened at certain wavelengths and this wavelength match the LEE peak. Therefore, the match of the reflectance and the LEE peak can prove that it is the interference effect that causes the enhancement of the light out-coupling efficiency. In additional, analytical method can be used to predict the location of OLED optimum efficiency. If a specific color OLED is provided, cavity thickness can be designed accordingly, such that the efficiency peak can match with the emission curve.

Chapter 6

HYPERBOLIC METAMATERIAL

6.1. Introduction

Hyperbolic Metamaterial is named due to the isofrequency contour inside this kind of structure. Figure 31 shows the isofrequency contour of wave vector k for (a) an isotropic dielectric and (b) (c) two types of anisotropic materials. The relationship between dielectric properties and wave vector is given by

$$\frac{k_x^2 + k_y^2}{\epsilon_{zz}} + \frac{k_z^2}{\epsilon_{xx}} = \frac{\omega^2}{c^2} \quad (30)$$

Note that a uniaxial crystal has the property of $\epsilon_{xx} = \epsilon_{yy} \neq \epsilon_{zz}$. In an isotropic material, where $\epsilon_{xx} = \epsilon_{zz}$, the k -space topology will be a sphere same as figure 31(a). In contrast, with extreme anisotropy that $\epsilon_{xx}\epsilon_{zz} < 0$, the isofrequency contour will be hyperboloid. There are two types of Hyperbolic Metamaterial (HMM). Type I HMM is when $\epsilon_{xx} = \epsilon_{yy} > 0$ and $\epsilon_{zz} < 0$. It has dielectric behavior on x, y directions and metallic behavior on z direction. On the other hand, type II HMM is opposite from type I HMM, where $\epsilon_{xx} = \epsilon_{yy} < 0$ and $\epsilon_{zz} > 0$. Substitute the dielectric properties into the equation above, a wave vector that is far exceeding the free space vector ($k_0 = \frac{\omega}{c}$) is derived. This phenomenon is also called high- k states. It allows the evanescent wave propagate within an HMM instead of exponentially decay away.

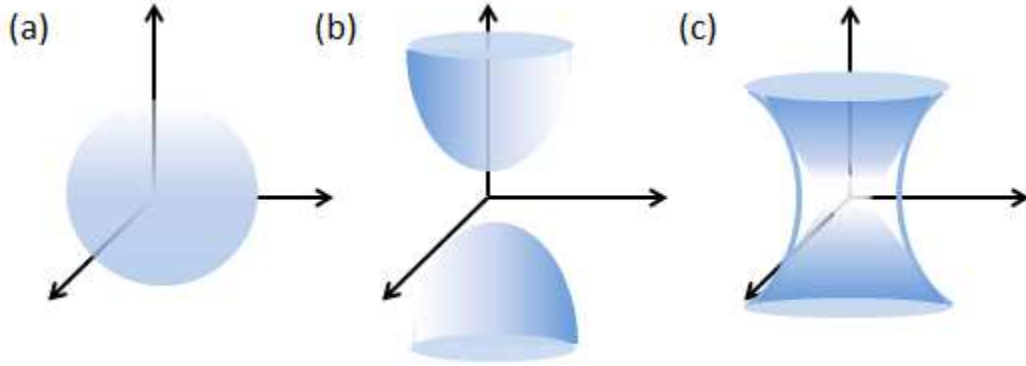


Figure 31: k-space Topology

To engineer the Hyperbolic Metamaterials, two methods can be used. One by building alternating layers of dielectric and metal as Figure 32. The other is to use metal nanowires inside dielectric host. Multilayer structure HMM is applied in this thesis. Cortes et al. suggested Au/TiO_2 and Ag/TiO_2 can be used for visible range. Because silver has lower loss compare to gold, Ag/TiO_2 is used as unit cell in the multilayers.

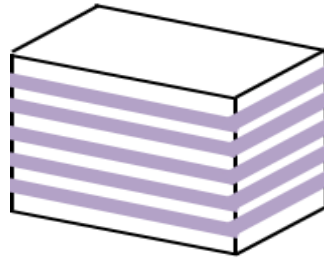


Figure 32: Schematic of Multilayer Hyperbolic Metamaterial

Effective Medium theory is introduced to calculate the dielectric properties of the HMM structure. This theory can be applied when the layer thicknesses is much smaller than the operating wavelength. In this case, ϵ_{xx} and ϵ_{zz} are given by

$$\begin{aligned}\epsilon_{xx} &= \rho\epsilon_m + (1 - \rho)\epsilon_d \\ \epsilon_{zz} &= \frac{\epsilon_m\epsilon_d}{\rho\epsilon_d + (1 - \rho)\epsilon_m}\end{aligned}\tag{31}$$

where ρ is the thickness of the metal to the thickness of unit cell, $\rho = \frac{t_m}{t_m + t_d}$. m refers

to metal and d refers to dielectric. Under the definition of type I and type II HMM, Figure 33 can be derived using EMT with Ag/ TiO_2 as unit cell.

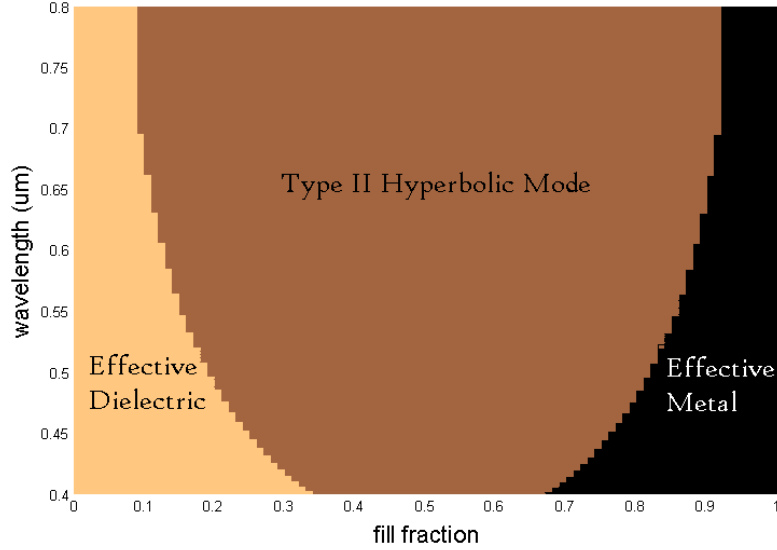


Figure 33: Material Type Predicted by Effective Medium Theory

Note that Effective dielectric is materials that have both ϵ_{xx} and ϵ_{zz} larger than zero, and effective metal indicates ϵ_{xx} and ϵ_{zz} are all smaller than zero. According to this result, a fill fraction of 0.5 is used to do the simulation.

6.2 Results and Analysis

Hyperbolic Metamaterial can be simulated in FDTD solutions as multilayer structures or by defining an anisotropic material using effective medium theory. The structure for this simulation contents 5 unit cells of Ag/ TiO_2 , the thicknesses of each layer are the same and equals to 5nm. Figure 34 shows the comparison results for these two methods. The blue and red line indicate the light extraction efficiency into the air, while green and black line show the extraction efficiency into the glass layer. It is

observed that the results from EMT and multilayer method are not perfectly match. This is due to inaccurate estimation of Effective Medium Theory. Kidwai et al. announced that EMT has a relatively poor accuracy when the emitting dipole is located closely to the Hyperbolic Metamaterial.

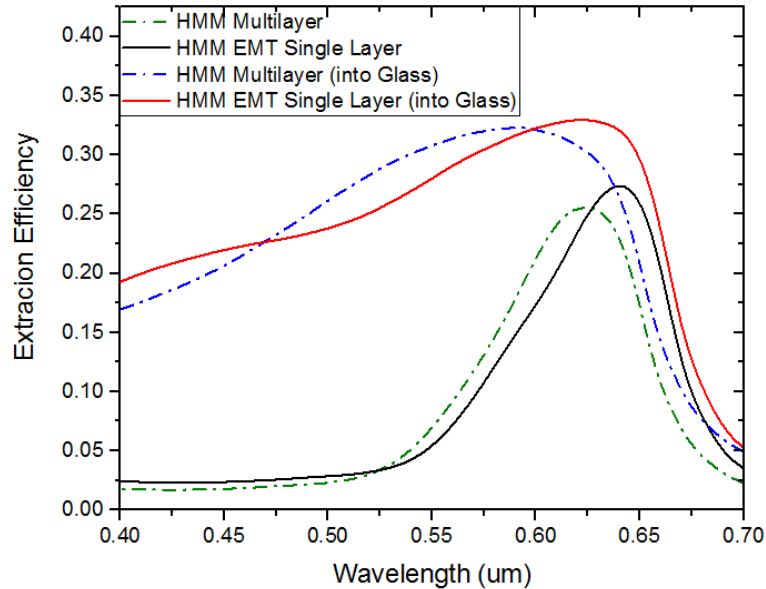


Figure 34: Simulation Results using Multilayer HMM and EMT Method HMM

Furthermore, as is indicated in Figure 35. Comparing the Hyperbolic Metamaterial with Fabry-Perot Structure, it is noticeable that the results turned out to be similar. Since 5 layers of 5 nm silver is included in the HMM structure, 25 nm Ag silver Fabry-Perot structure is used to make this comparison. The peak of light extraction efficiency occurs at the same wavelength of 625nm, indicating the same mechanism behind the results. In addition, the efficiency by Hyperbolic Metamaterial is slightly lower than that of Fabry-Perot structure. This is due to the total internal reflectance on several dielectric and metallic interfaces.

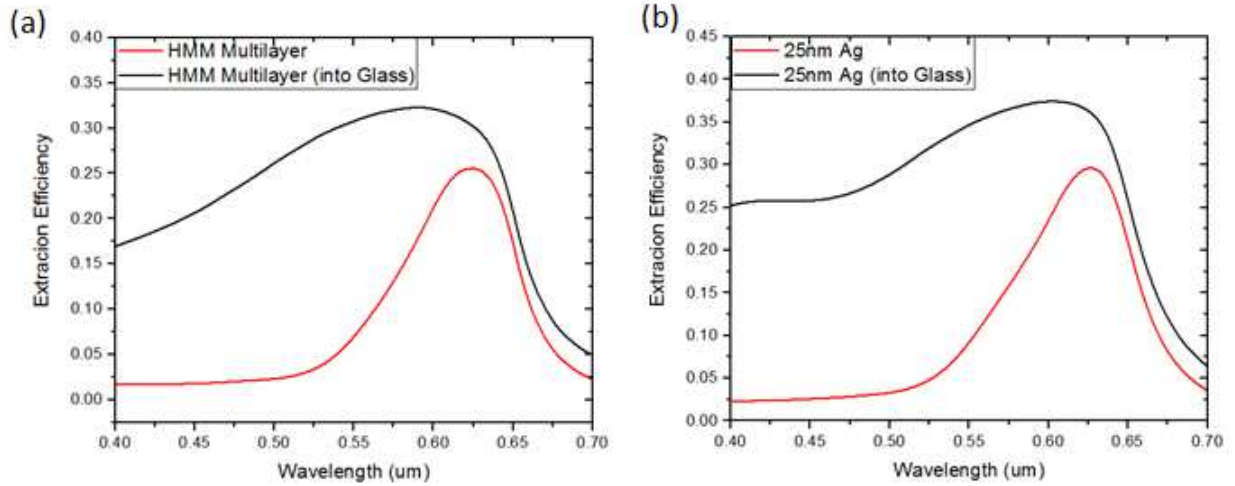


Figure 35: Comparison of Results from HMM Structure and Fabry-Perot Structure OLED

In conclusion, Hyperbolic Metamaterial is proved to have poor performance in Organic LED structure, as the emitting layer is so close to the HMM that the effective medium theory cannot be applied accurately.

Chapter 7

CONCLUSIONS AND FUTURE WORK

Proposed Organic LED structures have been evaluated by optical modeling in this study. The most promising structure is proved to be the Fabry-Perot cavity. With an ultrathin layer of silver as anode, maximum extraction efficiency is largely enhanced due to the interference effect. Optimization on the thickness of metal anode layer shows that 18nm silver gives the most efficient micro cavity structure. It is determined that this structure could concentrate the electric field within a small range of emitting angle, therefore avoid total internal reflectance loss within the structure. Furthermore, tune the thickness of NPD Layer could shift the optimum light extraction efficiency in spectrum. The peak of external quantum efficiency is red shift as NPD Layer gets thicker. With unpolarized light source and normal Aluminum cathode, 35% out-coupling efficiency is derived. Photonic Crystal structure, which optimum efficiency is 30%, also contributes to the enhancement of OLED efficiency. More pairs of unit cell in Photonic Crystal structure lead to narrow band of emission. Light from polarized light source in x-y orientation are more likely to extract out compare to light from z orientation light source. Engineering x-y polarized light source could enhance the efficiency by 50%. In addition, design cathode material similar to perfect reflector could eliminate the absorption loss in OLED devices. This method brings a further enhancement of 18% light extraction efficiency. In conclusion, an upper limit efficiency of 80% could be achieved by applying technologies above.

To facilitate future design, it is indicated in the study that Transfer Matrix Method can be chosen to predict the wavelength where the maximum extraction efficiency locates. Moreover, Hyperbolic Metamaterial is proved unfeasible in a thin OLED structure.

For future work, FDTD solutions will show more advantages when simulating 2D and 3D OLED structures. Plasmonic physical mechanism, which includes Surface Plasmon Polariton (SPP) and Magnetic Polariton (MP), could be utilized to further enhance the efficiency of OLED device. SPP and MP can be excited by building gratings structure, convex and concave structures. The challenge of design 2D and 3D OLED structure may include manufacturing difficulties and simulation accuracy which related to mesh size setting, convergence check, etc.. Nevertheless, modifying 3D structure Organic LEDs base on the results in this study may result in technical advances in near future.

REFERENCES

"How Much Electricity Is Used for Lighting in the United States?" U.S. Energy Information Administration. U.S. Department of Energy, 16 Apr. 2015. Web. 28 Nov. 2015.

"Halogen Lamp." Wikipedia. Wikimedia Foundation. Web. 15 Mar. 2016.

Pardo, Dino A.; Jabbour, G. E.; Peyghambarian, N. (2000). "Application of Screen Printing in the Fabrication of Organic Light-Emitting Devices". *Advanced Materials* 12 (17): 1249–1252. doi:10.1002/1521-4095(200009)12:17<1249::AID-ADMA1249>3.0.CO;2-Y

Saxena, Kanchan, V. K. Jain, and Dalip Singh Mehta. "A review on the light extraction techniques in organic electroluminescent devices." *Optical Materials* 32.1 (2009): 221-233.

Meerheim, Rico, Mauro Furno, Simone Hofmann, Björn Lüssem, and Karl Leo. "Quantification of Energy Loss Mechanisms in Organic Light-emitting Diodes." *Appl. Phys. Lett. Applied Physics Letters* 97.25 (2010): 253305. Web.

Patel, N.k., S. Cina, and J.h. Burroughes. "High-efficiency Organic Light-emitting Diodes." *IEEE J. Select. Topics Quantum Electron. IEEE Journal of Selected Topics in Quantum Electronics* 8.2 (2002): 346-61. Web.

Cheng, Yu-Hung, Jia-Lin Wu, Chien-Hong Cheng, Kao-Chih Syao, and Ming-Chang M. Lee. "Enhanced Light Outcoupling in a Thin Film by Texturing Meshed Surfaces." *Appl. Phys. Lett. Applied Physics Letters* 90.9 (2007): 091102. Web.

Ziebarth, J. M., A. K. Saafir, S. Fan, and M. D. McGehee. "Extracting Light from Polymer Light-Emitting Diodes Using Stamped Bragg Gratings." *Adv. Funct. Mater. Advanced Functional Materials* 14.5 (2004): 451-56. Web.

Wang, Z. B., M. G. Helander, J. Qiu, D. P. Puzzo, M. T. Greiner, Z. M. Hudson, S. Wang, Z. W. Liu, and Z. H. Lu. "Unlocking the Full Potential of Organic Light-emitting Diodes on Flexible Plastic." *Nature Photonics Nature Photon* 5.12 (2011): 753-57. Web.

Gou, Yuchun, and Yimin Xuan. "Role of metallic absorption on enhancing the light emitting efficiency by plasmonic gratings." *Journal of Applied Physics* 114.11 (2013): 113103.

Lumerical Inc. Simulation Methodology. Web. 10 June 2015. <http://docs.lumerical.com/en/index.html?oleds_simulation_methodology.html>.

"Photonic Crystal." Wikipedia. Wikimedia Foundation. Web. 15 Feb. 2016.

Ecton, Jeremy David. *Phosphorescent Organic Light Emitting Diodes Implementing Platinum Complexed*. Diss. Arizona State University, 2014.

Wang, L.p., B.j. Lee, X.j. Wang, and Z.m. Zhang. "Spatial and Temporal Coherence of Thermal Radiation in Asymmetric Fabry–Perot Resonance Cavities." *International Journal of Heat and Mass Transfer* 52.13-14 (2009): 3024-031. Web.

Frischeisen, Jörg, Daisuke Yokoyama, Ayataka Endo, Chihaya Adachi, and Wolfgang Brütting. "Increased Light Outcoupling Efficiency in Dye-doped Small Molecule Organic Light-emitting Diodes with Horizontally Oriented Emitters." *Organic Electronics* 12.5 (2011): 809-17. Web.

Mayr, Christian, Masatsugu Taneda, Chihaya Adachi, and Wolfgang Brütting. "Different Orientation of the Transition Dipole Moments of Two Similar Pt(II) Complexes and Their Potential for High Efficiency Organic Light-emitting Diodes." *Organic Electronics* 15.11 (2014): 3031-037. Web.

Kim, Kwon-Hyeon, Jae-Yeol Ma, Chang-Ki Moon, Jeong-Hwan Lee, Jang Yeol Baek, Yun-Hi Kim, and Jang-Joo Kim. "Controlling Emitting Dipole Orientation with Methyl Substituents on Main Ligand of Iridium Complexes for Highly Efficient Phosphorescent Organic Light-Emitting Diodes." *Advanced Optical Materials* 3.9 (2015): 1191-196. Web.

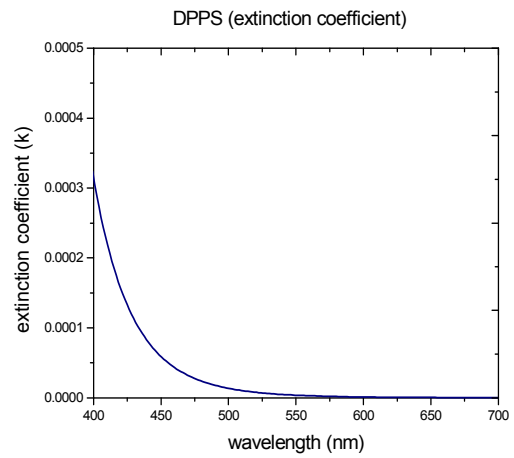
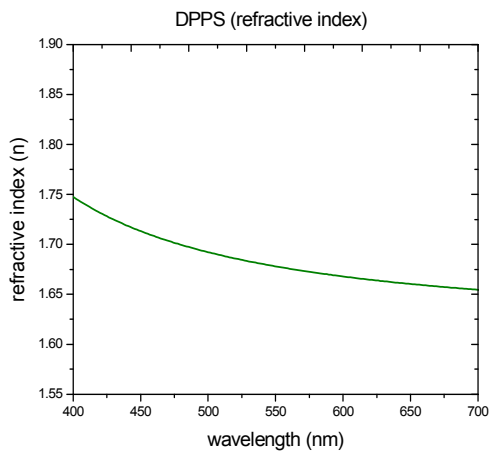
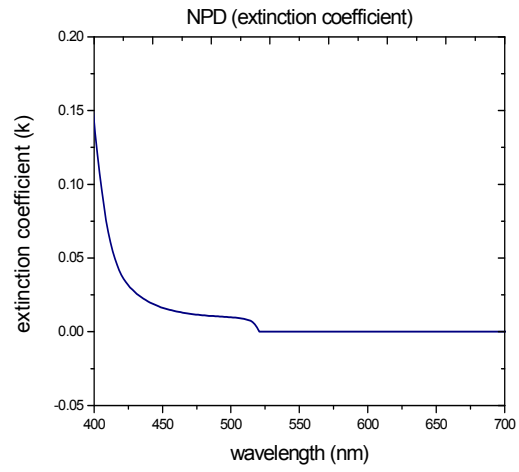
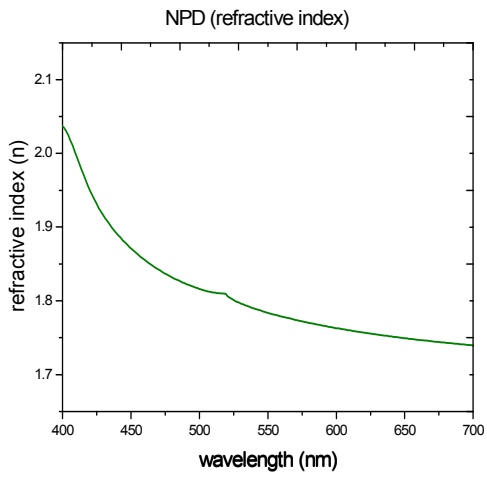
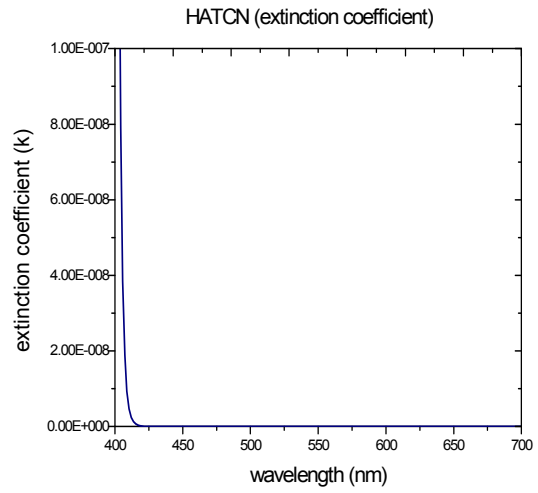
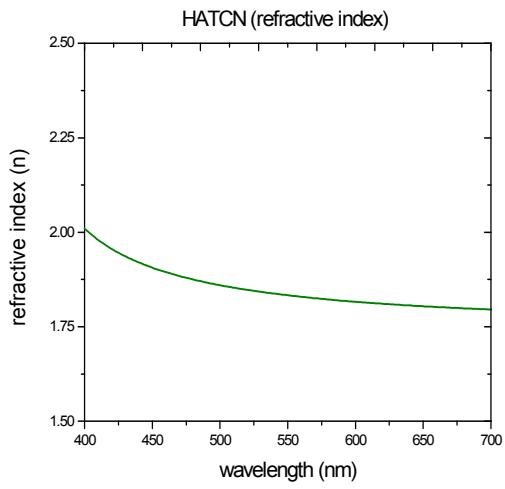
Zhang, Zhuomin M. *Nano/microscale Heat Transfer*. New York, NY: McGraw-Hill, 2007. Print.

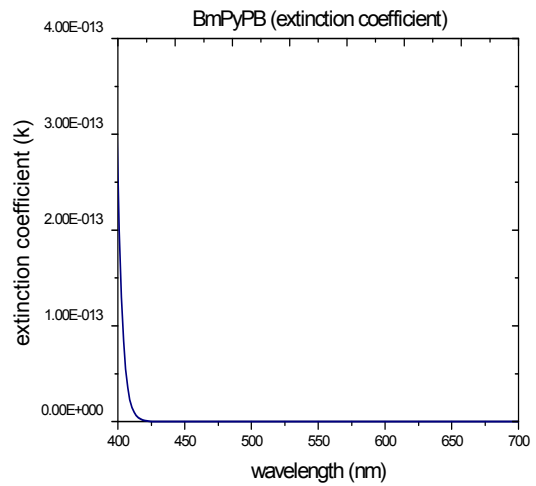
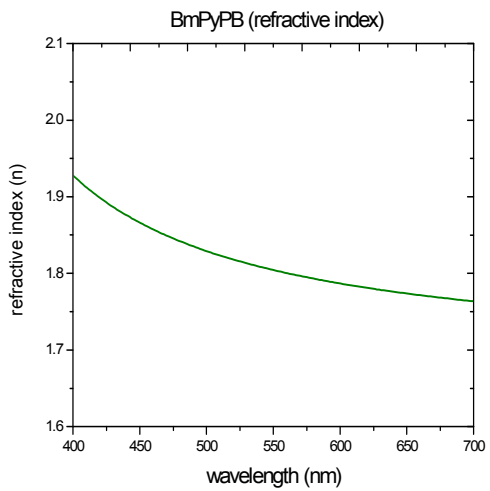
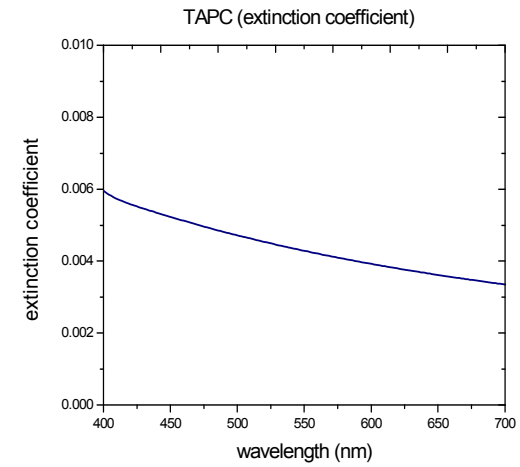
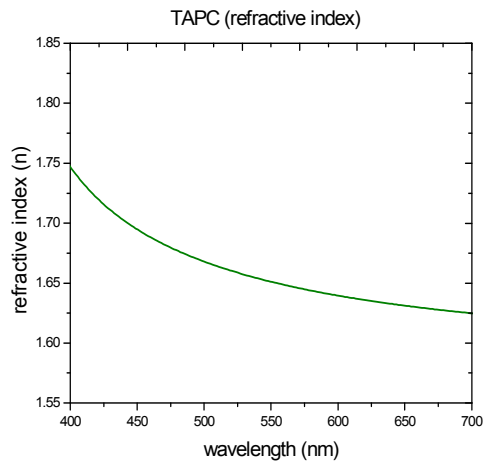
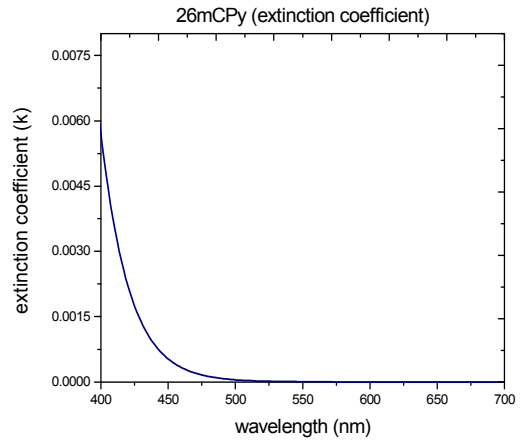
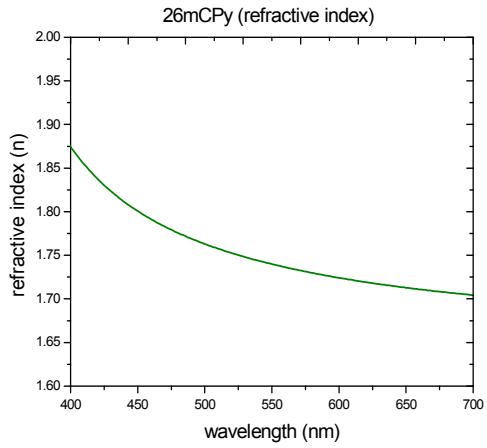
"Transfer Matrix Method." Wikipedia. Wikimedia Foundation. Web. 15 Feb. 2016.

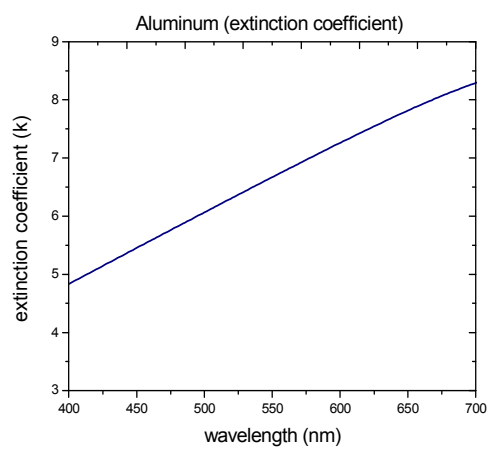
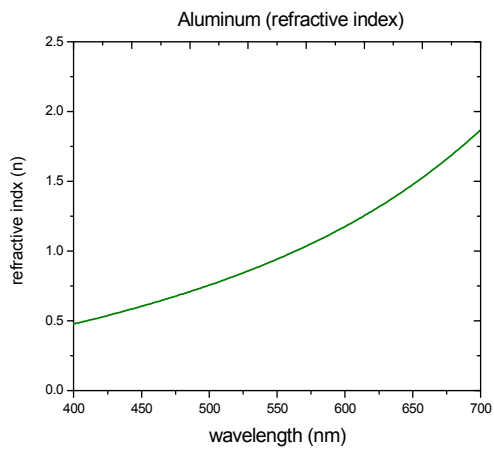
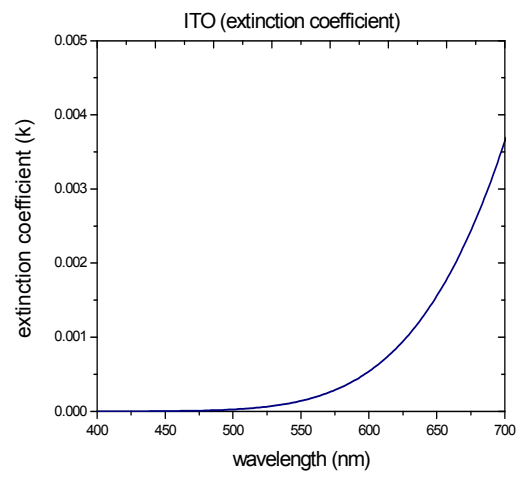
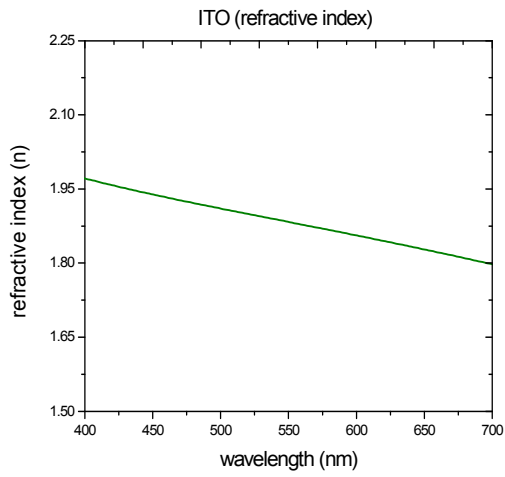
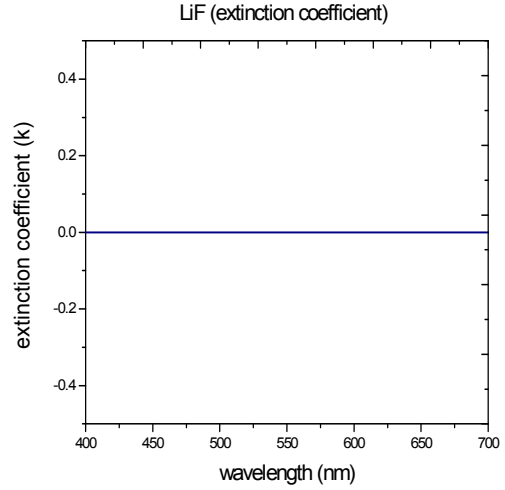
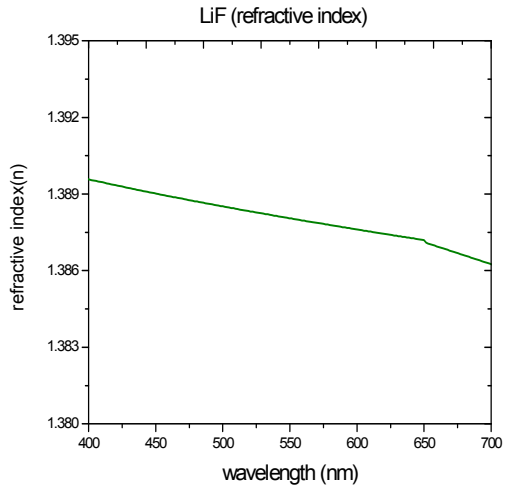
Wang, L. P., S. Basu, and Z. M. Zhang. "Direct and indirect methods for calculating thermal emission from layered structures with nonuniform temperatures." *Journal of Heat Transfer* 133.7 (2011): 072701.

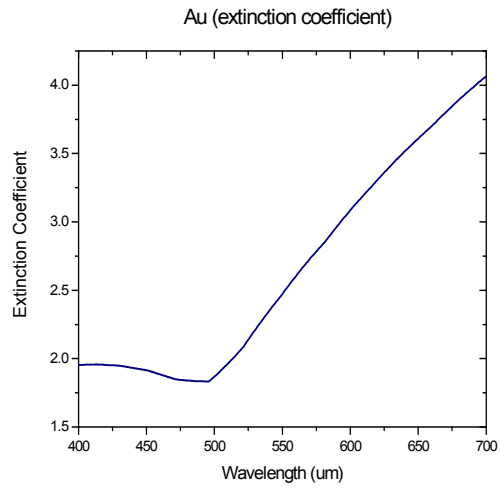
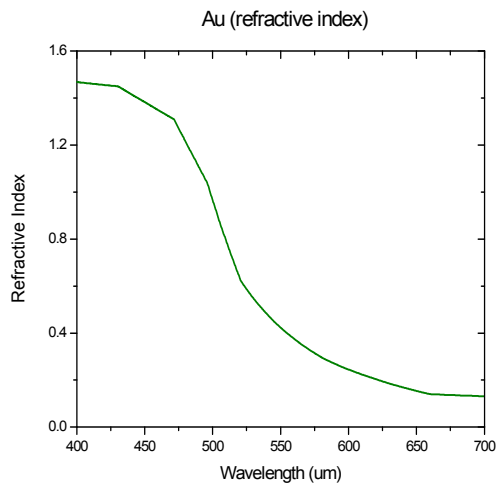
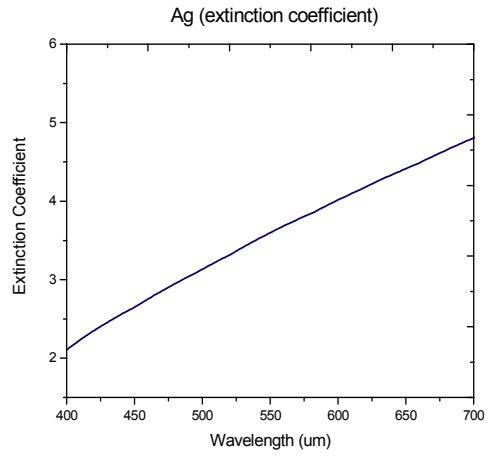
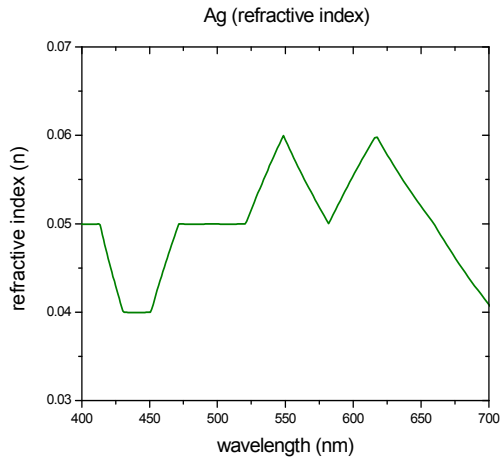
Omar Kidwat, * Sergei V. Zhukovsky. "Dipole radiation near hyperbolic metamaterials: applicability of effective-medium approximation." *optics letter*

APPENDIX A
MATERIAL PROPERTIES









APPENDIX B

FDTD CODE

B.1 MODEL SETUP

```
# px, py: location of the dipoles (fraction of unit cell)
# dipole_orientation: orientation of the dipole sources
```

```
select("source1");
if (dipole_orientation == "x"){
  set("theta",90);
  set("phi",0);
} else {
  if (dipole_orientation == "y"){
    set("theta",90);
    set("phi",90);
  } else {
    set("theta",0);
    set("phi",90);
  }
}
```

```
select("cathode");
set('x',0);
set('x span',xspan);
set('y',0);
set('y span',xspan);
set('z min',-0.5*10^-6);
set('z max',t_sub-0.5*10^-6);
```

```
select("LiF");
set('x',0);
set('x span',xspan);
set('y',0);
set('y span',xspan);
set('z max',t_sub-0.5*10^-6+t_LiF);
set('z min',t_sub-0.5*10^-6);
```

```
select("BmPyPB");
set('x',0);
set('x span',xspan);
set('y',0);
set('y span',xspan);
set('z min',t_sub-0.5*10^-6+t_LiF);
set('z max',t_BmPyPB+t_sub-0.5*10^-6+t_LiF);
```

```
select("DPPs");
set('x',0);
set('x span',xspan);
set('y',0);
set('y span',xspan);
```

```

set('z max',t_BmPyPB+t_sub-0.5*10^-6+t_LiF+t_DPPS);
set('z min',t_BmPyPB+t_sub-0.5*10^-6+t_LiF);

select("mCPy26");
set('x',0);
set('x span',xspan);
set('y',0);
set('y span',xspan);
set('z max',t_BmPyPB+t_sub-0.5*10^-6+t_LiF+t_DPPS+t_mCPy26);
set('z min',t_BmPyPB+t_sub-0.5*10^-6+t_LiF+t_DPPS);

select("TAPC");
set('x',0);
set('x span',xspan);
set('y',0);
set('y span',xspan);
set('z min',t_BmPyPB+t_sub-0.5*10^-6+t_LiF+t_DPPS+t_mCPy26);
set('z max',t_BmPyPB+t_sub-0.5*10^-6+t_LiF+t_DPPS+t_mCPy26+t_TAPC);

select("NPD");
set('x',0);
set('x span',xspan);
set('y',0);
set('y span',xspan);
set('z min',t_BmPyPB+t_sub-0.5*10^-6+t_LiF+t_DPPS+t_mCPy26+t_TAPC);
set('z
max',t_BmPyPB+t_sub-0.5*10^-
6+t_LiF+t_DPPS+t_mCPy26+t_TAPC+t_NPD);

select("HATCN");
set('x',0);
set('x span',xspan);
set('y',0);
set('y span',xspan);
set('z
min',t_BmPyPB+t_sub-0.5*10^-
6+t_LiF+t_DPPS+t_mCPy26+t_TAPC+t_NPD);
set('z
max',t_BmPyPB+t_sub-0.5*10^-
6+t_LiF+t_DPPS+t_mCPy26+t_TAPC+t_NPD+t_HATCN);

select("ITO");
set('x',0);
set('x span',xspan);
set('y',0);
set('y span',xspan);
set('z
min',t_BmPyPB+t_sub-0.5*10^-
6+t_LiF+t_DPPS+t_mCPy26+t_TAPC+t_NPD+t_HATCN);

```



```

        set('z', t_BmPyPB+t_sub-0.5*10^-
6+t_LiF+t_DPPS+t_mCPy26+t_TAPC+t_NPD+t_HATCN+t_ITO);

```

```

        select("glass");
        set('x',0);
        set('x span',xspan);
        set('y',0);
        set('y span',xspan);
        set('z', t_BmPyPB+t_sub-0.5*10^-
6+t_LiF+t_DPPS+t_mCPy26+t_TAPC+t_NPD+t_HATCN+t_ITO+t_glass);
        set('z', t_BmPyPB+t_sub-0.5*10^-
6+t_LiF+t_DPPS+t_mCPy26+t_TAPC+t_NPD+t_HATCN+t_ITO);

```

```

        select("source1");
        set('x', 0);
        set('y', 0);
        set('z', t_BmPyPB+t_sub-0.5*10^-
6+t_LiF+t_DPPS+t_mCPy26/2+dipole_location);

```

```

        # Set monitor box
        select("dipole_power");
        set('x',0);
        set('y',0);
        set('z',t_BmPyPB+t_sub-0.5*10^-
6+t_LiF+t_DPPS+t_mCPy26/2+dipole_location);
        select("mesh");
        set('x span',box_size);
        set('y span',box_size);
        set('z span',box_size);
        set('x',0);
        set('y',0);
        set('z',t_BmPyPB+t_sub-0.5*10^-
6+t_LiF+t_DPPS+t_mCPy26/2+dipole_location);

```

```

        select("far_field_change_index");
        set('x',0);
        set('y',0);
        set('y span',xspan);
        set('z',t_BmPyPB+t_sub-0.5*10^-
6+t_LiF+t_DPPS+t_mCPy26+t_TAPC+t_NPD+t_HATCN+t_ITO+20*10^-9);
        set('x span', xspan);
        set('y span', xspan);

```

```

        select('FDTD');
        set('x',0);

```

```

set('x span',domain_size);
set('y',0);
set('y span',domain_size);
set('z min',-0.2*10^-6);
set('z
max',t_BmPyPB+t_sub-0.5*10^-
6+t_LiF+t_DPPS+t_mCPy26+t_TAPC+t_NPD+t_HATCN+t_ITO+0.2*10^-6);

```

```

select('dipole_power');
set('x span',box_size);
set('y span',box_size);
set('z span',box_size);

```

B.2 FAR FIELD ANALYSIS GROUP

```

#####
# Do far field projection, accounting for fresnel
# reflections that occur at a far field interface.
#
# Input properties
# index_far: refractive index in the 'very far field'.
# In other words, the index beyond the far
# field interface. Should be a single real value (ie. non-dispersive, non-lossy)
# res: Resolution of the far field projection
#
# Output properties
# T_far: fraction of sourcepower transmitted to far field
# T_far1: transmission using default refractive index
# T_far2: transmission using 'index_far' refractive index
# T_near: the near field transmission. This should be equal
# to T_far1, but due to various numerical issues,
# it will not be exactly the same.
#
# E2_far: |E|^2 far field profile
# E2_far1: field profile using default refractive index
# E2_far2: field profile using 'index_far' refractive index
#
# Copyright 2012 Lumerical Solutions Inc
#####

if (havedata("index","index_x")) {
index_near = getdata("index","index_x");
} else {
index_near = getdata("index","index_z");
}

```

```

f=getdata("field","f");
nf=length(f);
T_near = transmission("field");

if (getdata("field","dimension")==3) {
# 3D analysis, assuming monitor is in XY plane

# Initialize variables
E2far1 = matrix(res,res,nf); # Electric far field in the material that the monitor is
located within. (standard far field projection)
E2far2 = matrix(res,res,nf); # Electric far field beyond the far field interface.
Power_far1 = matrix(nf); # Transmitted power in far field in default far field
material
Power_far2 = matrix(nf); # Transmitted power in far field beyond far field
interface

for (i=1:nf) {
# far field projection direction vectors
ux = farfieldux("field",i,res,res);
uy = farfielduy("field",i,res,res);
Ux=meshgridx(ux,uy);
Uy=meshgridy(ux,uy);
Uz=sqrt(1-Ux^2-Uy^2);
Theta = acos(Uz);

# Calculate electric field and transmitted power in far field, in the material that
the monitor is located within
EfarTemp = farfieldpolar3d("field",i,res,res);
E2far1(1:res,1:res,i) = abs(pinch(EfarTemp,3,2))^2 +
abs(pinch(EfarTemp,3,3))^2 ;
Power_far1(i) = 0.5*index_near(i)*sqrt(eps0/mu0) *
farfield3dintegrate(pinch(E2far1,3,i),ux,uy,90,0,0)/sourcepower(f(i));

# Calculate fresnel power transmission coefficients
Fresnel = stackrt([index_near(i); index_far],[0;0],f(i),Theta*180/pi);
Ts = reshape( Fresnel.Ts,[res,res] ); # reshape matrix; stackrt returns data as a
single vector rather than 2d matrix
Tp = reshape( Fresnel.Tp,[res,res] );
if (!finite(Ts)) { Ts(find(!finite(Ts))==1)=0; } # remove NAN's from matrix if they
happen to exist
if (!finite(Tp)) { Tp(find(!finite(Tp))==1)=0; }

# Calculate data beyond the far field interface, using Fresnel coefficients, snells
law, etc
# Note: The correct expression for the power in a unit of solid angle 3D is
# 0.5*sqrt(eps0/mu0)*n2*|E2|^2*dtheta2*dphi2*sin(theta2) =
0.5*sqrt(eps0/mu0)*n1* (Ts*|E1s|^2+Tp*|E1p|^2)*dtheta1*dphi1*sin(theta1)
# Remarkably, the sin(theta) that comes from the integration factor, multiplied
by the index that comes from

```

```

# getting the Poynting vector, cancel on either side since  $n_1 \sin(\theta_1) = n_2 \sin(\theta_2)$  by Snell's law.
# We also have  $d\phi_2 = d\phi_1$ .
# This leaves:
#  $|E_2|^2 = (T_s |E_{1s}|^2 + T_p |E_{1p}|^2) d\theta_1 / d\theta_2$ 
ux2 = ux * index_near(i)/index_far; # apply snells law
uy2 = uy * index_near(i)/index_far;
Ux2 = meshgridx(ux2,uy2);
Uy2 = meshgridy(ux2,uy2);
Uz2 = sqrt(1-Ux2^2-Uy2^2);
Theta2 = acos(Uz2);
Dtheta1_Dtheta2 = index_far*cos(Theta2)/(index_near(i)*cos(Theta)+1e-9); #
change of variables from ux,uy to ux2,uy2
Dtheta1_Dtheta2 = real(Dtheta1_Dtheta2);

E2farTemp = Ts * abs(pinch(EfarTemp,3,3))^2 + Tp *
abs(pinch(EfarTemp,3,2))^2; # apply fresnel coefficients
E2far2(1:res,1:res,i) = E2farTemp * Dtheta1_Dtheta2; # apply change of
variables factor

Power_far2(i) = 0.5*index_far*sqrt(eps0/mu0) *
farfield3dintegrate(pinch(E2far2,3,i),ux2,uy2,90,0,0)/sourcepower(f(i));

} # end loop over frequency

# Package results into datasets
T_far = matrixdataset("T_far");
T_far.addparameter("lambda",c/f,"f",f);
T_far.addattribute("T_far1",Power_far1);
T_far.addattribute("T_far2",Power_far2);
T_far.addattribute("T_near",T_near);

E2_far = matrixdataset("E2_far");
E2_far.addparameter("ux",ux);
E2_far.addparameter("uy",uy);
E2_far.addparameter("lambda",c/f,"f",f);
E2_far.addattribute("E2_far1",E2far1);
E2_far.addattribute("E2_far2",interp(E2far2,ux2,uy2,f,ux,uy,f));

} else {
# 2D analysis
# Initialize variables
E2far1 = matrix(res,nf); # Electric far field in the material that the monitor is
located within. (standard far field projection)
E2far2 = matrix(res,nf); # Electric far field beyond the far field interface.
Power_far1 = matrix(nf); # Transmitted power in far field in default far field
material

```

```

    Power_far2 = matrix(nf); # Transmitted power in far field beyond far field
interface

    for (i=1:nf) {
    # far field projection direction vectors
    theta = farfieldangle("field",i,res);

    # Calculate electric field and transmitted power in far field, in the material that
the monitor is located within
    EfarTemp = farfieldpolar2d("field",i,res);
    E2far1(1:res,i) = abs(pinch(EfarTemp,2,2))^2 + abs(pinch(EfarTemp,2,3))^2 ;
    Power_far1(i) = 0.5*index_near(i)*sqrt(eps0/mu0) *
farfield2dintegrate(pinch(E2far1,2,i),theta,90,0)/sourcepower(f(i));

    # Calculate fresnel power transmission coefficients
    Fresnel = stackrt([index_near(i); index_far],[0;0],f(i),theta);
    Ts = Fresnel.Ts;
    Tp = Fresnel.Tp;
    if (!finite(Ts)) { Ts(find(!finite(Ts))==1)=0; } # remove NAN's from matrix if they
happen to exist
    if (!finite(Tp)) { Tp(find(!finite(Tp))==1)=0; }

    # Calculate data beyond the far field interface, using Fresnel coefficients, snells
law, etc
    # Note: The correct expression for the power per angle in 2D is shown below.
Notice that the sin(theta)
    # is not present (compared to the 3D case) in the integration factor, so we have:
    #
    # 0.5*sqrt(eps0/mu0)*n1*(Ts*|E1s|^2+Tp*|E1p|^2)*dtheta1 =
0.5*sqrt(eps0/mu0)*n1*(Ts*|E1s|^2+Tp*|E1p|^2)*dtheta1
    # This leaves:
    # |E2|^2 = n1/n2*(Ts*|E1s|^2+Tp*|E1p|^2)*dtheta1/dtheta2
    # Interestingly, the n1/n2 does not cancel in 2D, since the sin(theta) term is not
present.
    theta2 = asin(index_near(i)/index_far*sin(theta*pi/180))*180/pi; # apply snells
law
    dtheta1_dtheta2 =
index_far*cos(theta2*pi/180)/(index_near(i)*cos(theta*pi/180)+1e-9); # change of
variables from theta to theta2
    dtheta1_dtheta2 = real(dtheta1_dtheta2);

    E2farTemp = index_near(i)/index_far * ( Ts * abs(pinch(EfarTemp,2,3))^2 + Tp
* abs(pinch(EfarTemp,2,2))^2 ); # apply fresnel coefficients
    E2far2(1:res,i) = E2farTemp * dtheta1_dtheta2; # apply change of variables
factor

    Power_far2(i) = 0.5*index_far*sqrt(eps0/mu0) *
farfield2dintegrate(pinch(E2far2,2,i),theta2,90,0)/sourcepower(f(i));

    } # end loop over frequency

```

```

# Remove data at complex angles (past 90)
pos = find(abs(theta2)<90);
theta2 = theta2(pos);
E2far2 = E2far2(pos,1:nf);

# Package results into datasets
T_far = matrixdataset("T_far");
T_far.addparameter("lambda",c/f,"f",f);
T_far.addattribute("T_far1",Power_far1);
T_far.addattribute("T_far2",Power_far2);
T_far.addattribute("T_near",T_near);

E2_far = matrixdataset("E2_far");
E2_far.addparameter("theta",theta);
E2_far.addparameter("lambda",c/f,"f",f);
E2_far.addattribute("E2_far1",E2far1);
E2_far.addattribute("E2_far2",interp(E2far2,theta2,f,theta,f));
}

```

B.3 BOX TRANSMISSION MONITOR

B.3.1 SETUP

```
deleteall;
#####
# Transmission box
# This script creates a box of monitors with a
# given x,y,z span
#
# Input properties
# x span, y span, z span: lengths of the rectangle
#
# Tags: transmission box power
#
# Copyright 2012 Lumerical Solutions Inc
#####

# simplify variable names by removing spaces
x_span = %x span%;
y_span = %y span%;
z_span = %z span%;

# add monitors
addpower; set("name", "x1");
addpower; set("name", "x2");
addpower; set("name", "y1");
addpower; set("name", "y2");
addpower; set("name", "z1");
addpower; set("name", "z2");

# set monitor orientation
selectpartial("x"); set("monitor type", "2D X-normal");
selectpartial("y"); set("monitor type", "2D Y-normal");
selectpartial("z"); set("monitor type", "2D Z-normal");

# set monitor positions
select("x1");
set("x", -x_span/2);
set("y", 0);
set("z", 0);
set("y span", y_span);
set("z span", z_span);
set('override global monitor settings', 1);
set('frequency points', points_num);

select("x2");
set("x", x_span/2);
```

```

set("y",0);
set("z",0);
set("y span",y_span);
set("z span",z_span);
set('override global monitor settings',1);
set('frequency points', points_num);

select("y1");
set("x",0);
set("y",-y_span/2);
set("z",0);
set("x span",x_span);
set("z span",z_span);
set('override global monitor settings',1);
set('frequency points', points_num);

select("y2");
set("x",0);
set("y",y_span/2);
set("z",0);
set("x span",x_span);
set("z span",z_span);
set('override global monitor settings',1);
set('frequency points', points_num);

select("z1");
set("x",0);
set("y",0);
set("z",-z_span/2);
set("x span",x_span);
set("y span",y_span);
set('override global monitor settings',1);
set('frequency points', points_num);

select("z2");
set("x",0);
set("y",0);
set("z",z_span/2);
set("x span",x_span);
set("y span",y_span);
set('override global monitor settings',1);
set('frequency points', points_num);

# disable z monitors in 2D simulations
selectpartial("z");
set("simulation type","3D");

# only record net power transmission, not field components
selectall;
set("output power",1);

```



```

set("output Ex",o);
set("output Ey",o);
set("output Ez",o);
set("output Hx",o);
set("output Hy",o);
set("output Hz",o);
set("output Px",o);
set("output Py",o);
set("output Pz",o);

```

B.3.2 CALCULATION SCRIPT

```

#####
# Transmission box
# This script calculates the net power out of the
# box of monitors. This script functions with symmetry
# boundary conditions, and in both 2D and 3D simulations
#
# Output properties
# T: power transmission flowing out of box
#
# Tags: transmission box power
#
# Copyright 2012 Lumerical Solutions Inc
#####

f=getdata("x2","f"); # get frequency data
dim = getdata("x2","dimension"); # dimension of simulation

Px2 = transmission("x2");
if(havedata("x1")){ Px1 = -transmission("x1"); } else { Px1=Px2; }
Py2 = transmission("y2");
if(havedata("y1")){ Py1 = -transmission("y1"); } else { Py1=Py2; }

# include z monitors if 3D simulation
if (dim==3) {
Pz2 = transmission("z2");
if(havedata("z1")){ Pz1 = -transmission("z1"); } else { Pz1=Pz2; }
} else {
Pz2 = 0; Pz1 = 0;
}

net_power = Px1 + Px2 + Py1 + Py2 + Pz1 + Pz2;

dp_box = net_power;
dp = dipolepower(f)/sourcepower(f);

```

```

sp = sourcepower(f);

T = matrixdataset("T");
T.addparameter("lambda",c/f,"f",f);
T.addattribute("T",net_power);

dipole_power = matrixdataset("dipole_power");
dipole_power.addparameter("lambda",c/f,"f",f);
dipole_power.addattribute("dipole_power",dp); # actual power radiated as
measured by dipolepower function, normalized to source power (power radiated by
dipole in homogeneous material)
dipole_power.addattribute("dipole_power_box",dp_box); # actual power
radiated as measured by box, normalized to source power (power radiated by dipole in
homogeneous material)
dipole_power.addattribute("source_power",sp); # power radiated radiated by
dipole in homogeneous material, in Watts

```

B.4 SWEEP TOOL SCRIPT

```

# Uncomment this line to run the parameter sweep from this script
# runsweep; save;
# Get no pattern results
# Gett pattern results
T_far = getsweepresult("pattern_dipole_position","T_far_avg");
dipolePower = getsweepresult("pattern_dipole_position","dipolePower_avg");
f = T_far.f;
# calculate transmission into 5 deg cone normal to the surface
ext_enhancement_5_deg = matrix(length(f));
half_angle = 5;
# for the patterned case, plot fraction of power transmitted
# into the air, trapped in the glass substrate, and trapped
# in the OLED structure
Power_total = dipolePower.dipole_power / dipolePower.dipole_power;
Power_air = T_far.T_far2 / dipolePower.dipole_power;
Power_glass = (T_far.T_far1-T_far.T_far2) / dipolePower.dipole_power;
Power_OLED = Power_total - Power_air-Power_glass;

#### plot results ####

# For patterned structure, plot the fraction of power lost in each region:
# OLED thin layers, Glass or Air. Sum of these values is 1.
plot(c/f*1e6,Power_total,real(Power_air),
real(Power_glass),real(Power_OLED),
"wavelength(um)","Fraction of emitted power","Patterned OLED");
legend("Total","Air","Glass","OLED");

```